



1

1 **Enhanced representation of soil NO emissions in the**
2 **Community Multi-scale Air Quality (CMAQ) model**

3 **Quazi Z. Rasool¹, Rui Zhang¹, Benjamin Lash^{1*}, Daniel S. Cohan¹, Ellen Cooter²,**
4 **Jesse Bash² and Lok N. Lamsal^{3,4}**

5 [1]{Department of Civil and Environmental Engineering, Rice University, Houston, Texas, USA}

6 [2]{Computational Exposure Division, National Exposure Research Laboratory, Office of Research and
7 Development, US Environmental Protection Agency, RTP, NC, USA}

8 [3]{Goddard Earth Sciences Technology and Research, Universities Space Research Association,
9 Columbia, MD 21046, USA }

10 [4]{NASA Goddard Space Flight Center, Greenbelt, MD 20771, USA}

11 [*]{now at: School of Natural Sciences, University of California, Merced, CA}

12 *Correspondence to:* Daniel Cohan (cohan@rice.edu)

13

1



14 **Abstract**

15 Modeling of soil nitric oxide (NO) emissions is highly uncertain and may misrepresent its spatial
16 and temporal distribution. This study builds upon a recently introduced parameterization to
17 improve the timing and spatial distribution of soil NO emission estimates in the Community
18 Multi-scale Air Quality (CMAQ) model. The parameterization considers soil parameters,
19 meteorology, land use, and mineral nitrogen (N) availability to estimate NO emissions. We
20 incorporate daily year-specific fertilizer data from the Environmental Policy Integrated Climate
21 (EPIC) agricultural model to replace the annual generic data of the initial parameterization, and
22 use a 12 km resolution soil biome map over the continental US. CMAQ modeling for July 2011
23 shows slight differences in model performance in simulating fine particulate matter and ozone
24 from IMPROVE and CASTNET sites and NO₂ columns from Ozone Monitoring Instrument
25 (OMI) satellite retrievals. We also simulate how the change in soil NO emissions scheme affects
26 the expected O₃ response to projected emissions reductions.



27 **1 Introduction**

28 Nitrogen oxides ($\text{NO}_x = \text{NO} + \text{NO}_2$) play a crucial role in tropospheric chemistry. Availability of
29 NO_x influences the oxidizing capacity of the troposphere as NO_x directly reacts with hydroxyl
30 radicals (OH) and catalyzes tropospheric ozone (O_3) production and destruction (Seinfeld and
31 Pandis, 2012). NO_x also affects the lifetime of reactive greenhouse gases like CH_4 by influencing
32 its dominant oxidant OH (Steinkamp and Lawrence, 2011), thus affecting the Earth's radiative
33 balance (IPCC, 2007). NO_x also influences rates of formation of inorganic particulate matter
34 (PM) (Wang et al., 2013) and organic PM (Seinfeld and Pandis, 2012).

35 Soil NO_x emissions accounts for ~15-40 % of the tropospheric NO_2 column over the continental
36 United States (CONUS), and up to 80% in highly N fertilized rural areas like the Sahel of Africa
37 (Hudman et al., 2012). The estimated amount of nitric oxide (NO) emitted from soils is highly
38 uncertain, ranging from 4-15 Tg-N yr^{-1} , with different estimates of total global NO_x budget also
39 showing a mean difference of 60-70% (Potter et al., 1996; Davidson and Kinglerlee, 1997;
40 Yienger and Levy, 1995; Jaeglé et al., 2005; Stavrakou et al., 2008; Steinkamp and Lawrence,
41 2011; Miyazaki et al., 2012; Stavrakou et al., 2013; Vinken et al., 2014). Soil NO_x is mainly
42 emitted as NO through both microbial activity (biotic/enzymatic) and chemical (abiotic/non-
43 enzymatic) pathways, with emission rates varying as a function of meteorological conditions,
44 physicochemical soil properties, and nitrogen (N) inputs from deposition and fertilizer or manure
45 application (Pilegaard, 2013; Hudman et al., 2012). The fraction of soil N emitted as NO varies
46 with meteorological and soil conditions such as temperature, soil moisture content, and pH
47 (Ludwig et al., 2001; Parton et al., 2001; van Dijk et al., 2002; Stehfest and Bouwman, 2006).

48 Different biome types, comprised of vegetation and soil assemblages exhibit different NO
49 emission factors under different soil conditions and climate zones. One of the early attempts to
50 stratify soil NO based on different biomes by Davidson and Kinglerlee (1997) involved
51 compiling over 60 articles and 100 field estimates. They clearly identified biomes associated
52 with low NO emissions like swamps, tundra, and temperate forests, and those with high soil NO
53 fluxes like tropical savanna/woodland and cultivated agriculture. For instance, high soil NO
54 fluxes were observed in croplands, savannahs or woodlands, N-rich temperate forests and even
55 boreal/tropical forests with low NO_2^- availability in warm conditions and acidic soil (Kesik et
56 al., 2006; Cheng et al., 2007; Su et al., 2011). This approach, however, fails to capture within-



4

57 biome variation in NO emissions (Miyazaki et al., 2012; Vinken et al., 2014). Steinkamp and
58 Lawrence (2011) more recently compiled worldwide emission factors from a dataset consisting
59 of 112 articles with 583 field measurements of soil NO_x covering the period from 1976 to 2010,
60 and regrouped them into 24 soil biome type based on MODIS land cover category as well as
61 Köppen climate zone classifications (Kottek et al., 2006).

62 N deposition can be a significant driver of soil NO emissions in N-limited settings or near strong
63 N emissions sources, where both wet and dry deposition of N species act like an additional
64 fertilizer source (Yienger and Levy, 1995; Hudman et al., 2012). The response of soil NO_x
65 emission to N deposition varies as a function of soil N status and land-use history of the land
66 use/biome type. Mature forests for instance with already high initial soil N due to higher
67 mineralization rates give higher soil NO flux than rehabilitated and disturbed ones (Zhang et al.,
68 2008). In agricultural soils, N deposition is a leading contributor to the inorganic N pool that
69 eventually contributes to soil NO emissions (Liu et al., 2006; Pilegaard, 2013).

70 Fertilizer (organic and inorganic) application represent controllable influences on soil N
71 emissions (Pilegaard, 2013) and are leading sources of reactive nitrogen (N) worldwide
72 (Galloway and Cowling, 2002). U.S. fertilizer use increased by nearly a factor of 4 from 1961 to
73 1999 (IFIA, 2001). Soil NO emissions increase with rising fertilizer application, with conversion
74 rate of applied fertilizer N to NO_x being up to ~ 11% (Williams et al., 1988; Shepherd et al.,
75 1991). Open and closed chamber studies have shown increasing fertilizer application to increase
76 both NO and N₂O fluxes simultaneously, but with variability in NO/N₂O emission ratio
77 (Harrison et al., 1995; Conrad, 1996; Veldkamp and Keller, 1997).

78 Meteorological conditions influence soil NO emission rates. Large pulses of biogenic NO
79 emissions often follow the onset of rain after a dry period (Davidson, 1992; Scholes et al., 1997;
80 Jaeglé et al., 2004; Hudman et al., 2010). Soil NO pulsing events occur when water stressed
81 nitrifying bacteria, which remain dormant during dry periods, are activated by the first rains and
82 start metabolizing accumulated N in the soil. NO pulses of up to 10–100 times background levels
83 typically last for about 1–2 days (Yienger and Levy, 1995; Hudman et al., 2012).

84 Adsorption onto plant canopy surfaces can reduce the amount of soil NO emissions entering the
85 broader atmosphere. Yienger and Levy (1995) (YL) soil NO scheme followed a Canopy
86 Reduction Factor (CRF) approach (Wang et al., 1998) to account for the reduction of soil NO

4



87 emission flux *via* stomatal or cuticle exchange as a function of dry deposition within the canopy
88 on a global scale.

89 Contemporary air quality models such as the Community Multi-scale Air Quality (CMAQ)
90 model most often use an adaptation of the YL scheme to quantify soil NO emissions as a
91 function of fertilizer application, soil moisture, precipitation and CRF (Byun and Schere, 2006).
92 However, YL has been found to underestimate emissions rates inferred from satellite and ground
93 measurements by a factor ranging from 1.5 to 4.5, and to misrepresent some key spatial and
94 temporal features of emissions (Jaeglé et al., 2005; Wang et al., 2007; Boersma et al., 2008; Zhao
95 and Wang, 2009; Lin, 2012; Hudman et al., 2012; Vinken et al., 2014). This overall
96 underestimation can be attributed to several uncertainties in the modeling settings, such as
97 inaccurate emissions coefficients, poor soil moisture data, deriving soil temperatures from
98 ground air temperatures, neglecting nitrogen deposition and outdated fertilizer application rates
99 (Yienger and Levy, 1995; Jaeglé et al., 2005; Delon et al., 2007; Wang et al., 2007; Boersma et
100 al., 2008; Delon et al., 2008; Hudman et al., 2010; Steinkamp and Lawrence, 2011; Hudman et
101 al., 2012).

102 The Berkley Dalhousie Soil NO Parameterization (BDSNP) scheme, originally implemented by
103 Hudman et al. (2012) in the GEOS-Chem global chemical transport model, outperforms YL by
104 better representing biome type, the timing of emissions, and actual soil temperature and moisture
105 (Hudman et al., 2010).

106

107 Our approach builds upon BDSNP by using the Environmental Policy Integrated Climate (EPIC)
108 biogeochemical model for dynamic representation of the soil N pool on a day-to-day basis. EPIC
109 is a field scale biogeochemical process model developed by the United States Department of
110 Agriculture (USDA) to represent plant growth, soil hydrology, and soil heat budgets for multiple
111 soil layers of variable thickness, multiple vegetative systems and crop management practices
112 (Cooter et al., 2012). EPIC can model up to 1 sq. km (100 ha) spatially and on a daily time scale
113 (CMAS, 2015). EPIC simulations are compatible with spatial and temporal scale of CMAQ as
114 well (Bash et al., 2013). EPIC accounts for different agricultural management scenarios, accurate
115 simulation of soil conditions and plant growth to produce plan demand-driven fertilizer estimates
116 for BDSNP (Cooter et al., 2012; Bash et al., 2013).



117 Baseline soil NO emission rate for each location (Hudman et al., 2012; Vinken et al., 2014), use
118 a new soil biome map with finer-scale representation of land cover systems consistent with
119 typical resolution of a regional model. We also built an offline version of BDSNP (stand-alone
120 BDSNP), which can use benchmarked inputs from the CMAQ and allows quick diagnostic based
121 on soil NO estimates for sensitivity analysis (Supplementary material Section S.2).

122

123

124 **2 Methodology**

125

126 **2.1 Implementation of advanced soil NO parameterization in CMAQ**

127 **2.1.1 Land surface model (LSM)**

128 Our implementation of the BDSNP soil NO parameterization in CMAQ uses Pleim-Xiu Land
129 Surface Model (Pleim and Xiu, 2003). Compared to the coarser LSM in GEOS-Chem (Bey et al.,
130 2001), Pleim-Xiu provides finer-scale estimates of soil moisture and soil temperature based on
131 solar radiation, temperature, Leaf Area Index (LAI), vegetation coverage, and aerodynamic
132 resistance. The rich amount of information available from the Pleim-Xiu LSM enables refined
133 representation of soil moisture and soil temperature for implementation in soil NO
134 parameterization.

135 **2.1.2 Canopy reduction factor**

136 The original implementation of BDSNP in GEOS-Chem did not provide specific spatial-
137 temporal variation of CRF in each modeling grid, but used a monthly average CRF from Wang
138 et al. (1998). Wang et al. (1998) included an updated CRF as part of their implementation of YL
139 into GEOS-Chem. This CRF is based on wind speed, turbulence, canopy structure, deposition
140 constants, and other physical variables. In the GEOS-Chem implementation of BDSNP, this CRF
141 reduced the flux by $\sim 16\%$, from $10.7 \text{ Tg-N yr}^{-1}$ above soil to 9 Tg-N yr^{-1} above canopy
142 (Hudman et al., 2012).



143 Our BDSNP implementation for CMAQ uses the same approach of integrating CRF as used in
144 Wang et al. (1998) with the biome categorization based on Steinkamp and Lawrence (2011) and
145 Köppen climate classes (Kottek et al. 2006) in the soil NO_x parametrization itself.

146 **2.1.3 Fertilizer**

147 YL in CMAQ assumed a linear correlation between fertilizer application and its induced
148 emissions over general growing season, May-August in the Northern Hemisphere and
149 November-February in the Southern Hemisphere (Yienger and Levy, 1995) rather than peaking
150 near the time of fertilization at the beginning of the local growing season. This likely caused
151 inaccurate temporal representation of fertilizer driven emissions in certain regions (Hudman et
152 al., 2012). The GEOS-Chem implementation of BDSNP applied a long-term average fertilizer
153 application with a decay term after fertilizer is applied. Constant fertilizer emissions neglect an
154 important phenomenon: applying fertilizer during a dry period when neither plants nor bacteria
155 may have the water available to use it may result in a large pulse when the soil is eventually re-
156 wetted (Pilegaard, 2013). Such dry spring N fertilizer application can be quite significant,
157 especially in the mid-west and southern plains in the US (Cooter et al., 2012). The current
158 fertilizer data used for the BDSNP is scaled to global 2006 emissions by Hudman et al. (2012)
159 using a spatial distribution for year 2000 from Potter et al. (2010). This global database reported
160 by Potter et al. (2010) is already 8 years out of date in magnitude and 14 years out of date for
161 relative distribution, and has relatively coarse resolution based on out-of-date long term average
162 (national-level fertilizer data from 1994 to 2001). Using recent fertilizer application information
163 is essential to soil NO estimates given the fact that N fertilizer is the major contributor to plant
164 nutrient use in US, and its share has been increasing from 11,535 thousand short tons in 2001 to
165 12,840,000 short tons in 2013 (USDA ERS, 2013). Our implementation of BDSNP into CMAQ
166 is designed to enable updates by subsequent developers to use new year- and location- specific
167 fertilizer data. We use the Fertilizer Emission Scenario Tool for CMAQ (FEST-C v1.1,
168 <http://www.emascenter.org>) to incorporate EPIC fertilizer application data into our CMAQ runs.

169 **2.1.4 N Deposition**



170 YL in CMAQ neglects nitrogen deposition, which can result in an 0.5 Tg/yr underestimation in
171 soil NO_x globally (~5%) (Hudman et al., 2012). The implementation of the EPIC model in
172 FEST-C inputs oxidized and reduced form of N deposition directly into soil ammonia and nitrate
173 pools each day. In Our implementation of BDSNP, these daily time series derive from previous
174 CMAQ simulation. Inclusion of this deposition N source acts to reduce the simulated plant-
175 based demand for additional N applications.

176 **2.1.5 Formulation of soil NO scheme**

177 Figure 1 provides the flow chart of the BDSNP scheme implementation, which has the option to
178 run in-line with CMAQ, or offline as a stand-alone emissions parameterization. Static input files
179 in Hudman et al. 2012 BDSNP implementation (labelled as ‘old’ in Fig. 1) such as those giving
180 soil biome type with climate zone and global fertilizer pool are needed to determine the soil base
181 emission value at each modeling grid. The Meteorology-Chemistry Interface Processor (MCIP)
182 (Otte and Pleim, 2010) takes outputs from a meteorological model such as Weather Research and
183 Forecasting (WRF) model (Skamarock et al., 2008) to provide a complete set of meteorological
184 data needed for emissions and air quality simulations.

185 There are seven key input environment variables and two key output environment variables in
186 our implementation of BDSNP. Table S1 lists their names and corresponding functionalities.

187 Our implementation of the BDSNP soil NO_x emission, S_{NO_x} in CMAQ multiplies a base
188 emission factor (A) by scaling factors dependent on soil temperature (T) and soil moisture (θ),
189 i.e., $f(T)$, $g(\theta)$ and a pulsing term (P) (equation 1). The base emission factor depends on biome
190 type under wet or dry soil conditions. The pulsing term depends on the length of the dry period,
191 rather than the accumulated rainfall amount considered by YL. The CRF term estimate the
192 fractional reduction in soil NO_x flux due to canopy resistance.



$$193 \quad S_{NO_x} Flux \left(\frac{ng N}{m^2 s} \right) =$$

$$194 \quad A'_{biome} (N_{avail}) \times f(T) \times g(\theta) \times P(l_{dry}) \times CRF(LAI, Meteorology, Biome) \quad (1)$$

$$195 \quad A'_{biome} = A_{biome} + N_{avail} \times \bar{E} \quad (2)$$

$$196 \quad N_{avail}(t) = N_{avail Fert}(0) \times e^{-\frac{t}{\tau_1}} + F \times \tau_1 \times \left(1 - e^{-\frac{t}{\tau_1}} \right) + N_{avail Dep}(0) \times e^{-\frac{t}{\tau_2}} + D \times \tau_2 \times$$

$$197 \quad \left(1 - e^{-\frac{t}{\tau_2}} \right)$$

$$198 \quad (3)$$

199 Fertilizer and deposition both contribute to modifying the A'_{biome} emissions coefficients for each
 200 biome. Available nitrogen (N_{avail}) at time t from fertilizer and deposition is multiplied by
 201 emission rate, \bar{E} , based on the observed global estimates of fertilizer emissions ($\sim 1.8 \text{ Tg-N yr}^{-1}$)
 202 by Stehfest and Bouwman (2006) and added to biome specific soil NO emission factors (A_{biome})
 203 from Steinkamp and Lawrence (2011) to give the net base emission factor (A'_{biome}) (Eq. (2) and
 204 Eq. (3)). The resulting A' is multiplied by the meteorological scaling or response factors: $f(T)$,
 205 $g(\theta)$, and $P(l_{dry})$ as in Eq. (1). The soil temperature response or scaling factor $f(T)$ is simplified to
 206 be exponential everywhere. NO flux now depends on soil moisture (θ) instead of rainfall, and it
 207 increases smoothly to a maximum value before decreasing as the ground becomes water
 208 saturated. In Eq. (3), F is fertilization rate (kg ha^{-1}), D is the wet and dry deposition rate (kg ha^{-1})
 209 considered as an additional fertilization rate, and τ is decay time, which is 4 months for fertilizer
 210 (τ_1) and 6 months for deposition (τ_2) (Hudman et al. 2012).

211 BDSNP uses a Poisson function to represent the dependence of emission rates on soil moisture
 212 (θ), where the parameters ' a ' and ' b ' vary for different climates such that the maximum of the
 213 function occurs at $\theta = 0.2$ for arid soils and $\theta = 0.3$ otherwise (Hudman et al. 2012). We adopt
 214 the same approach in CMAQ, as follows:

$$215 \quad f(T) * g(\theta) = e^{0.103 * T} * a * \theta * e^{-b * \theta^2} \quad (4)$$

216 The pulsing term depends on the length of the dry period (l_{dry}) and a change in soil moisture
 217 instead of on the amount of precipitation (Hudman et al., 2012).



218 The pulsing term for emissions when rain follows a dry period is

$$219 \quad P(l_{dry}, t) = [13.01 * \ln(l_{dry}) - 53.6] * e^{-c*t} \quad (5)$$

220 In this equation, l_{dry} is the length of the dry period that preceded the rain and $c = 0.068 \text{ hour}^{-1}$
221 defines the exponential decay of the pulse.

222 Beyond this basic implementation of the above stated BDSNP framework into CMAQ, there
223 were major modifications (highlighted as ‘new’ in Fig. 1) in the form of: a) updating biome map
224 consistent with CMAQ, b) incorporating year- and location- specific fertilizer data using EPIC
225 outputs and c) development of a standalone BDSNP module. Our work focuses on those
226 developments discussed in detail in the sections to follow.

227

228 **2.2 Soil biome map over CONUS**

229 The original implementation of BDSNP used the global soil biome data from the GEOS-Chem,
230 with emission factors for each biome under dry/wet conditions taken from Steinkamp and
231 Lawrence (2011) (Appendix Table A1). Our implementation in CMAQ uses a finer resolution
232 (12 km) soil biome map over CONUS. The map is generated from the 30-arc-second
233 (approximately 1 kilometer) NLCD40 (National Land Cover Dataset) for 2006, with 40 land
234 cover/land use classifications. A mapping algorithm table (see Appendix Table A2) was created
235 to connect the land use category to soil biome type (Table A1) based on best available
236 knowledge. For the categories with identical names, such as ‘evergreen needleleaf forest’,
237 ‘deciduous needleleaf forest’, ‘mixed forest’, ‘savannas’ and ‘grassland’, the mapping is direct.
238 Categories in NLCD40, which are subsets of the corresponding biome category, are consolidated
239 into one category by addition. For example, ‘permanent snow and ice’ and ‘perennial ice-snow’
240 in NLCD40 are combined to form ‘snow and ice’; ‘developed open space’, ‘developed low
241 intensity’, ‘developed medium intensity’, and ‘developed high intensity’ are added to form
242 ‘urban and built-up lands’. For the categories appearing only in NLCD40, the mapping algorithm
243 is determined by referring to the CMAQ mapping scheme, available in Cross-Section and
244 Quantum Yield (CSQY) data files in the CMAQ coding. One such case is to map ‘lichens’ and



245 ‘moss’ in NLCD40 to the category ‘grassland’ in soil biome. Furthermore, a model resolution
246 compatible Köppen climate zone classification (Kottek et al., 2006) was added to allocate
247 different emission factor for the same biome type e.g. to account for different altitudes of
248 ‘grassland’ at different locations. There are five climate zone classifications, namely A:
249 equatorial, B: arid, C: warm temperature, D: snow, E: polar. A 12 km CONUS model resolution
250 climate zone classification map (see Figure 2) was created using the Spatial Allocator based on
251 the county level climate zone definition as the surrogate based on a dominant land use,
252 (<http://koeppen-geiger.vu-wien.ac.at/data/KoeppenGeiger.UScounty.txt>).

253 Figure 2 compares the 24 soil biome map with 0.25 degree resolution from the GEOS-Chem
254 settings to the new 12 km resolution soil biome map we created here for CMAQ. Table A2 gives
255 the biome type names with corresponding climate zones.

256 The classification of simulation domain into arid and non-arid region with consistent resolution
257 is also included in our implementation. Figure B1 shows the distribution of arid (red) and non-
258 arid (blue) regions. For the modeling grid classified as ‘arid’ region, the maximum moisture
259 scaling factor corresponds to the water-filled pore space (θ) value equal to 0.2; while for the
260 ‘non-arid’ modeling grid, the maximum moisture scaling factor corresponds with $\theta=0.3$
261 (Hudman et al., 2012).

262 **2.3 Representation of fertilizer N**

263 We implemented two approaches for representing fertilizer N. The first approach regrids
264 fertilizer data from the global GEOS-Chem BDSNP implementation (Hudman et al. 2012) to our
265 12 km resolution CONUS domain. That scheme uses the global fertilizer database from Potter et
266 al. (2010) and assumed 37% of fertilizer and manure N is available (1.8 Tg-N yr^{-1}) for potential
267 emission. Figure B2 provides the day-by-day variation of total N remaining due to fertilizer
268 application over CONUS during a year, and shows the typical cycle between growing season and
269 non-growing season. The Potter data, however, are a decade old and at coarse resolution for
270 county-level in US.

271 Our second approach (Figure 3) uses the EPIC model as implemented in the FEST-C tool
272 (Cooter et al. 2012) to provide a dynamic representation of fertilizer applications for a specific
273 growing season. FEST-C (v1.1) generates model-ready fertilizer input files for CMAQ. . Use of



274 FEST-C/EPIC instead of soil emissions from YL scheme has been shown to improve CMAQ
275 performance for nitrate and ammonia in CONUS (Bash et al., 2013). The BELD4 tool in FEST-
276 C system was used to provide the crop usage fraction over our domain. We summed FEST-C
277 data for ammonia, nitrate and organic, T1_ANH3, T1_ANO3 and T1_AON respectively in kg-
278 N/ha, to give a total soil N pool for each of 42 simulated crops (CMAS, 2015). This daily crop-
279 wise total soil N pool was then weighted by the fraction of each crop type at each modeling grid
280 to get a final weighted sum total soil N pool usable in BDSNP. CMAQ v.5.0.2 can be run with
281 in-line biogenic emissions, calculated in tandem with the rest of the model. Since the EPIC N
282 pools already include N deposition, we designed our soil NO emissions module to be flexible in
283 recognizing whether it is using fertilizer data such as Potter et al. (2010) that does not include
284 deposition or EPIC that does.

285 Figure 4 compares the FEST-C derived N fertilizer map and the default coarser resolution long-
286 term average fertilizer map from Potter. While the spatial patterns are similar, EPIC provides
287 finer resolution and more up-to-date information.

288

289 **2.4 Model configurations and data use for model evaluations**

290 The CMAQ domain settings for CONUS as provided by the EPA were used to simulate the
291 whole month of July in 2011. July corresponds to the month of peak flux for soil nitrogen
292 emissions in the United States (Williams et al., 1992; Cooter et al., 2012; Bash et al., 2013) and
293 is an active period for ozone photochemistry (Cooper et al., 2014; Strode et al., 2015).

294 A ten day (21 June-30 June, 2011) spin-up time was used to minimize the influence from initial
295 conditions. The domain consisted of 396 columns, 246 rows, 26 vertical layers, and 12 km
296 rectangular cells using a Lambert Conformal Projection over North America. This configuration
297 was consistent throughout the WRF-BDSNP-CMAQ modeling framework (see Figure 1).
298 Meteorology data were produced through the WRF Model nudged to National Centers for
299 Environmental Prediction (NCEP) and National Center for Atmospheric Research Reanalysis
300 (NARR) data, which is comprised of historical observations and processed to control quality and
301 consistency across years by National Oceanic and Atmospheric Administration (NOAA).



302 Emissions were generated using the Sparse Matrix Operator Kernel Emissions (SMOKE) model
303 (CMAS, 2014) and 2011NEIv1.

304

305 We applied CMAQ with three sets of soil NO emissions: a) Standard YL soil NO scheme, b)
306 BDSNP scheme with Potter et al. (2010) fertilizer data set and biome mappings from GEOS-
307 Chem, and c) BDSNP scheme with EPIC 2011 data and new biome mappings. Within these
308 three cases, we simulated the impact of anthropogenic NO_x reductions applied to all contributing
309 source sectors listed in the 2011 National Emission Inventory (NEI). For this purpose, we
310 considered the baseline NO_x reduction scenario from 2011 to 2025 that EPA's Regulatory
311 Impact Analysis (RIA) determined for Business as Usual (BAU) in the CONUS domain (Figure
312 2A-1, Table 2A-1 in <https://www3.epa.gov/ttn/ecas/docs/20151001ria.pdf>). Table 1 gives a full
313 list of modeling configurations settings used for achieving the above-mentioned simulations.

314 Model simulations were evaluated against the following in situ and satellite-based data: 16
315 USEPA Clean Air Status and Trends Network (CASTNET) sites for MDA8 O₃
316 (www.epa.gov/castnet), 9 Interagency Monitoring of Protected Visual Environments
317 (IMPROVE) sites for daily average PM_{2.5} (Malm et al., 1994), and NASA's OMI retrieval
318 product for tropospheric NO₂ column (Bucsela et al., 2013; Lamsal et al., 2014). Fig. 5 shows the
319 spatial distribution of the ground sites used for validation of modeled estimates. The selected
320 ground sites for model validation are mostly based in agricultural regions with intense fertilizer
321 application rate and high NO fluxes, specifically the Midwest, southern plains, and San Joaquin
322 Valley.

323

324 We also simulated three sensitivity cases for the same time period and domain with the offline
325 soil NO module: a) NLCD40 based (new) biome vs GEOS-Chem based (old) biome (using EF1
326 in Table A1), b) EPIC 2011 vs Potter data and, c) Global mean biome emission factor (EF1 in
327 Table A1) vs North American mean emission factor (EF3 in Table A1) (Supplementary material
328 Section S.3).

329



330 **3 Results and Discussion**

331 **3.1 Spatial distribution of nitrogen fertilizer application and soil NO** 332 **emissions over CONUS**

333 We demarcated the CONUS domain into six sub-domains (Figure 6) to analyze model outputs.
334 The updated BDSNP model and EPIC fertilizer result in higher soil NO emission rates than YL
335 and Potter. Emissions increase by a factor ranging from 1.8 to 2.8 in shifting from YL to
336 BDSNP, even while retaining the Potter fertilizer data and original biome map, indicating that
337 the shift from YL to BDSNP scheme is the largest driver of the increase in emissions estimates.
338 EPIC and the new biome dataset further increase emissions over most of CONUS, except for the
339 southwest region. In Midwest and Western US, the new biome map identified more cropland and
340 shifted some grasslands to other land cover types such as forests, savannah and croplands, which
341 exhibit higher soil NO emissions (Figure 2; Table A1). The Midwest region is characterized with
342 the highest emission rate due to its abundant agricultural lands with high fertilizer application
343 rates (Figure 4).

344 **3.2 Evaluation of CMAQ NO₂ with satellite OMI NO₂ observations**

345 The standard (version 2.1) OMI tropospheric NO₂ column observations from NASA's Aura
346 satellite as discussed in Bucsele et al. (2013) and Lamsal et al. (2014) were used for comparison
347 with our modelled NO₂ vertical columns. To enable comparison, the quality-assured, clear-sky
348 (cloud radiance fraction < 0.5) OMI NO₂ data were gridded and projected to our domain by
349 using ArcGIS 10.3. CMAQ modelled NO₂ column densities in molecules per cm² were derived
350 using vertical integration and extracted for 13:00-14:00 local time, corresponding to the time of
351 OMI measurements.

352 We compared CMAQ simulated tropospheric NO₂ columns with OMI product for regions
353 showing highest sensitivity in soil NO switching from YL to BDSNP: Midwest, San Joaquin
354 Valley in California and central Texas (see Appendix Figure B3). Switching from YL to our
355 updated BDSNP ('new') module improved agreement with OMI NO₂ columns in central Texas



356 but over-predicts column NO₂ in the San Joaquin Valley and Midwest (Figure 7). Even the YL
357 estimate was higher than OMI by a factor of two in the Midwest (Figure 7).

358 **3.3 Evaluation with PM_{2.5} and ozone observations**

359 Model results are compared with observational data from IMPROVE monitors for PM_{2.5} and
360 CASTNET monitors for ozone. We first compute differences between ozone and PM_{2.5} estimates
361 from the three simulation cases to identify sites influenced by the choice of soil NO scheme
362 during our July 2011 episode (Figures 8 and 9). These highlights nine IMPROVE sites for PM_{2.5}
363 and 16 CASTNET sites for ozone (Figures 5, 8 and 9) where CMAQ results are sensitive to soil
364 NO changes (Figure 6).

365 Statistical comparisons of modeled and observed daily average PM_{2.5} at the nine IMPROVE sites
366 are provided in Table 2. Mean Absolute Gross Error (MAGE) and Root Mean Square Error
367 (RMSE) improved from 2.8 to 2.7 ug/m³ and 3.4 to 3.3 ug/m³ respectively when moving from
368 YL to BDSNP with the new inputs. Both Pearson's and Spearman's ranked correlation
369 coefficient (R) shows no significant change when soil NO module in CMAQ is switched from
370 YL to BDSNP (Potter with old biome) and BDSNP (EPIC with new biome) (Tables 2). Use of
371 the ranked correlation coefficient minimizes the impact of spurious correlations due to outliers
372 but does not affect the analysis. Switching from YL to our updated BDSNP ('new') module
373 shows that the predicted versus observed fit becomes slightly closer to 1:1 (Figure 10).
374 Numerical Mean Bias (NMB) and Numerical Mean Error (NME) improve from -28.5% to -
375 26.4% and 34.6% to 33.6%, respectively.

376 In contrast to the PM_{2.5} results, the updated soil NO scheme yields mixed impacts on model
377 performance for maximum daily average 8-hour (MDA8) ozone at the targeted 16 CASTNET
378 sites (Table 3 and Figure 11). For the 11 agricultural/prairie sites, replacement of YL with
379 BDSNP with new inputs increases NMB from 7.6% to 14.1% and NME from 15.7 to 19.3%
380 (Table 3). The excess ozone may occur because FEST-C does not account for the loss of
381 fertilizer N to the water stream ("tile drainage") in wet conditions (Dinnes et al., 2002). Hudman
382 et al. (2012) suggested $\theta = 0.175$ (m³/m³) as threshold below which dry condition occur. During
383 July 2011, in Midwest monthly mean soil moisture (θ_{mean} , m³/m³) is mostly > 0.175 , indicating



384 possibility of wet conditions (Fig. S5). This can also be due to known wet bias in WRF simulated
385 meteorology i.e. more perceived precipitation than observed (Zhang et al., 2009) which may
386 result in high NO emissions in moist soils. Overestimation of O₃ is due to higher NO emissions,
387 as these regions comprise of mostly NO_x limited rural locations.

388 At the California CASTNET sites, BDSNP enhances model performance in simulating observed
389 MDA8 ozone (Table 3). This can be seen in the NMB, NME, MAGE, and RMSE comparisons
390 between YL and BDSNP, though updating BDSNP to the newer inputs does not enhance
391 performance (Table 3).

392 **3.4 Impact of soil NO scheme on ozone sensitivity to anthropogenic NO_x** 393 **perturbations**

394 We analyzed how the choice of soil NO parameterization affects the responsiveness of ozone to
395 reductions in anthropogenic NO_x emissions. We applied emission perturbation factors based on
396 the 5.7 million ton reduction in baseline anthropogenic NO_x emissions from 2011 to 2025 that
397 US EPA simulated in its latest RIA (U.S. EPA, 2015). Table 4 gives the perturbation factors we
398 used to obtain baseline anthropogenic NO_x emissions for 2025 over all contributing sectors as
399 listed from NEI 2011. Since our simulation is for July 2011 over CONUS, we used these
400 perturbation factors rather than the net reductions in RIA to scale emissions in a similar pattern
401 as given in RIA for annual baseline perturbations from 2011 to 2025 with BAU.

402

403 Shifting from YL to the BDSNP soil NO scheme reduces the sensitivity of MDA8 O₃ to
404 anthropogenic NO_x perturbations. The impacts are greatest in California and the Midwest, where
405 shifting to BDSNP can reduce the expected impact of the anthropogenic NO_x reductions by ~ 1
406 to 1.5 ppbV. Changing the inputs within the BDSNP scheme has a smaller impact (Figure 12).
407 Our results imply that the higher soil NO emissions from our updated BDSNP module shifts the
408 ozone photochemistry to a less strongly NO_x-limited regime.

409



410 **4 Conclusions**

411 Our BDSNP implementation represents a substantial update from the YL scheme for estimating
412 soil NO in CMAQ. Compared to the previous implementation of BDSNP in global GEOS-Chem
413 model, our implementation in CMAQ incorporated finer-scale representation of its dependence
414 on land use, soil conditions, and N availability. This finer resolution and updated biome and
415 fertilizer data set resulted in higher sensitivity of soil NO to biome emission factors. Our updated
416 BDSNP scheme (EPIC and new biome) predicts slightly higher soil NO than the inputs used in
417 GEOS-Chem, primarily due to the use of 2011 daily EPIC/FEST-C fertilizer data and fine
418 resolution NLCD40 biomes (Figure 6).

419 Sensitivities to different input datasets were examined using our standalone BDSNP module to
420 reduce computational cost. Switching from GEOS-Chem biome to new NLCD40 biome drops
421 soil NO in the northwest and southwest portions of our domain due to the finer resolution biome
422 map exhibiting lower emission factors in those regions. Replacing fertilizer data from Potter et
423 al. (2010) with an EPIC 2011 dataset increased soil NO mostly in the Midwest (Supplementary
424 material Figure S4).

425 We compared tropospheric NO₂ column densities output from our CMAQ runs with the three
426 inline soil NO schemes to OMI observations as spatial average over regions sensitive to switch
427 from YL to our updated BDSNP scheme. Temporal average of OMI and CMAQ simulated NO₂
428 column densities was done over the OMI overpass time (13:00-14:00 local time) for July 2011
429 monthly mean. Figure 7 summarizes tropospheric NO₂ column density comparisons between
430 model and OMI satellite observation for aforementioned sensitive regions. Central Texas showed
431 improvement with switch from YL to our BDSNP ('new') scheme. For July 2011, central Texas
432 and San Joaquin Valley exhibit relatively dry soil conditions, whereas the Midwest was mostly
433 wet (Supplementary material Figure S5). Even with similar conditions as central Texas, San
434 Joaquin region shows overall degradation. Overestimation of simulated NO₂ columns up to twice
435 of OMI over Midwestern US and San Joaquin valley for summer episodes has been exhibited
436 earlier as well (Lamsal et al., 2014). Several factors, such as spatial inhomogeneity within OMI
437 pixels and possible errors arising from the stratosphere-troposphere separation scheme and air
438 mass factor calculations, can be attributed to this overestimation. Retrieval difficulties in
439 complex terrain may explain the discrepancies in NO₂ column over San Joaquin Valley even



440 though it shows slight improvement with updates within BDSNP ('old' to 'new') and has similar
441 dry conditions as central Texas.

442 We examined the performance of CMAQ under each of the soil NO parameterizations. Regions
443 where soil NO parameterizations most impacted MDA8 ozone and PM_{2.5} were examined for
444 model performance in simulating CASTNET MDA8 O₃ and IMPROVE PM_{2.5} observations.

445 For PM_{2.5}, our updated BDSNP module ('new') showed the best performance (Table 2).
446 Evaluations against MDA8 O₃ observations found contrasting behavior for two different sets of
447 CASTNET sites. The 11 mostly agricultural and prairie sites extending across the Midwest and
448 southern US showed consistent overestimation as we moved from YL to BDNBP with new
449 inputs, with bias jumping from ~ 7% to 14% and error from 15% to 19% (Table 3). However, the
450 5 forest/national park sites most of which lie near the San Joaquin Valley by contrast showed an
451 overall improvement in bias from ~ 13% to 10% and in error from ~ 17 % to 15% (Table 3).

452 Over-predictions of soil NO emissions especially in wet conditions may result from EPIC not
453 properly accounting for on-farm nitrogen management practices like tile drainage. Crops such as
454 alfalfa, hay, grass, and rice experience soil N loss due to tile drainage in wet soils (Gast et al.,
455 1978; Randall et al., 1997). Recent updates to FEST-C (v. 1.2) include tile drainage for some
456 crops but not hay, rice, grass and alfalfa (CMAS, 2015). Tile drainage results in loss of fertilizer
457 N to water run-off from wet or moist soils.

458 We analyzed how the soil NO schemes affect the sensitivity of MDA8 ozone to anthropogenic
459 NO_x reductions by considering the 5.7 million tons/year reduction from 2011 levels that U.S.
460 EPA expects for United States by 2025 with BAU scenario. These reductions were applied on
461 basis of perturbation factors of relevant sectors keeping biogenic emissions unchanged for July
462 2011, based on EPA's annual baseline estimates between 2011 and 2025 (Table 4). These
463 anthropogenic NO_x reductions yield less reduction in MDA8 O₃ under the BDNBP soil NO
464 scheme than YL, with 1-2 ppbv differences over parts of California and the Midwest (Figure 12).
465 The shift occurs because our updated BDSNP schemes have higher soil NO in these regions,
466 pushing them toward less strongly NO_x-limited regimes.



467 This work represents crucial advancement toward enhanced representation of soil NO in a
468 regional model. Although possible wet biases and using dominant land cover rather than
469 fractional in soil biome classification, may have over-predicted NO in agricultural regions in
470 present study. The EPIC simulation used here lacks complete representation of farming
471 management practices like tile, which can reduced soil moisture and soil NO fluxes. Inclusion of
472 biogeochemistry influencing different reactive N species encompassing the entire N cycling
473 could enable more mechanistic representation of emissions. For future work, there is a need for
474 more accurate representation of actual farming practices and internalizing updated soil reactive N
475 bio-geochemical schemes. More field observations are needed as well in order to increase the
476 sample size for evaluation of modeled estimates soil emissions of reactive N species beyond NO.

477

478 **Code availability**

479 The modified and new scripts used for implementation of BDSNP in CMAQ Version 5.0.2 are in
480 the supplementary material. Also provided as supplement is the user manual giving details on
481 implementing BDSNP module in-line with CMAQ, as used in this work. Source codes for
482 CMAQ version 5.0.2 and FEST-C version 1.1 are both open-source, available with applicable
483 free registration at <http://www.cmascenter.org>. Advanced Research WRF model (ARW) version
484 3.6.1 used in this study is also available as a free open-source resource at
485 http://www2.mmm.ucar.edu/wrf/users/download/get_source.html.

486 **Acknowledgements**

487 This work was supported by NASA's Air Quality Applied Sciences Team through a tiger team
488 project grant for DYNAMO: DYnamic Inputs of Natural Conditions for Air Quality Models.
489 Although this work was reviewed by EPA and approved for publication, it may not necessarily
490 reflect official Agency policy.

491



492 **References**

- 493 Bash, J., Cooter, E., Dennis, R., Walker, J., and Pleim, J.: Evaluation of a regional air-quality model with
494 bidirectional NH₃ exchange coupled to an agroecosystem model, *Biogeosciences*, 10, 1635-1645, 2013.
- 495 Bey, I., Jacob, D. J., Yantosca, R. M., Logan, J. A., Field, B., Fiore, A. M., Li, Q., Liu, H., Mickley, L. J., and
496 Schultz, M.: Global modeling of tropospheric chemistry with assimilated meteorology: Model description
497 and evaluation, *J. Geophys. Res.*, 106, 23,073-23,096, 2001.
- 498 Boersma, K., Jacob, D. J., Bucsel, E., Perring, A., Dirksen, R., Yantosca, R., Park, R., Wenig, M., Bertram,
499 T., and Cohen, R.: Validation of OMI tropospheric NO₂ observations during INTEX-B and application to
500 constrain NO_x emissions over the eastern United States and Mexico, *Atmospheric Environment*, 42,
501 4480-4497, 2008.
- 502 Bucsel, E. J., Krotkov, N. A., Celarier, E. A., Lamsal, L. N., Swartz, W. H., Bhartia, P. K., Boersma, K. F.,
503 Veefkind, J. P., Gleason, J. F., and Pickering, K. E.: A new stratospheric and tropospheric NO₂ retrieval
504 algorithm for nadir-viewing satellite instruments: applications to OMI, *Atmos. Meas. Tech.*, 6, 2607-
505 2626, doi:10.5194/amt-6-2607-2013, 2013.
- 506 Byun, D. W. and Schere, K. L.: Review of the governing equations, computational algorithms, and other
507 components of the models- 3 Community Multiscale Air Quality (CMAQ) modeling system, *Appl. Mech.*
508 *Rev.*, 59, 51-77, 2006.
- 509
- 510 Conrad R. Soil microorganisms as controllers of atmospheric trace gases (H₂, CO, CH₄, OCS, N₂O, and
511 NO). *Microbiological Reviews*. 60(4):609-640; 1996.
- 512 Cooper, O.R., Parrish, D.D., Ziemke, J., Balashov, N.V., Cupeiro, M., Galbally, I.E., Gilge, S., Horowitz, L.,
513 Jensen, N.R., Lamarque, J.F. and Naik, V.: Global distribution and trends of tropospheric ozone: An
514 observation-based review. *Elementa: Science of the Anthropocene*, 2(1), p.000029, 2014.
- 515 Cheng, J.-l., Zhou, S., and Zhu, Y.-w.: Assessment and mapping of environmental quality in agricultural
516 soils of Zhejiang Province, China, *Journal of Environmental Sciences*, 19, 50-54, 2007.
- 517 CMAS, Sparse Matrix Operators Kernel Emissions model (SMOKE) version 3.6, University of North
518 Carolina at Chapel Hill Institute for the Environment, Center for Environmental Modeling for Policy



- 519 Development (CEMPD), Community Modeling and Analysis System Center (CMAS), Chapel Hill, NC
520 (<http://www.smoke-model.org>), 2014.
- 521 CMAS 2015: User's Guide for the Fertilizer Emission Scenario Tool for CMAQ (FEST-C) Version 1.2,
522 Institute of Environment, The University of North Carolina at Chapel Hill, Chapel Hill, NC, available at:
523 https://www.cmascenter.org/fest-c/documentation/1.2/FESTC1_2_userManual.pdf, last accessed: 30
524 September, 2015
- 525 Cooter, E. J., Bash, J.O., Benson, V., and Ran, L.: Linking agricultural crop management and air quality
526 models for regional to national-scale nitrogen assessments. *Biogeosciences*, 9, no. 10: 4023-4035, 2012.
- 527 Davidson, E.: Pulses of nitric oxide and nitrous oxide flux following wetting of dry soil: an assessment of
528 probable sources and importance relative to annual fluxes, *Ecol. Bull.*, 42, 149–155, 1992.
- 529 Davidson, E. and Kinglerlee, W.: A global inventory of nitric oxide emissions from soils, *Nutr. Cycl.*
530 *Agroecosys.*, 48, 37–50, doi:10.1023/A:1009738715891, 1997.
- 531 Delon, C., Serça, D., Boissard, C., Dupont, R., Dutot, A., Laville, P., De Rosnay, P., and Delmas, R.: Soil NO
532 emissions modelling using artificial neural network, *Tellus B*, 59, 502-513, 2007.
- 533 Delon, C., Reeves, C., Stewart, D., Serça, D., Dupont, R., Mari, C., Chaboureaud, J.-P., and Tulet, P.:
534 Biogenic nitrogen oxide emissions from soils—impact on NO_x and ozone over West Africa during AMMA
535 (African Monsoon Multidisciplinary Experiment): modelling study, *Atmospheric Chemistry and Physics*,
536 8, 2351-2363, 2008.
- 537 Dinnes, D. L., Karlen, D. L., Jaynes, D. B., Kaspar, T. C., Hatfield, J. L., Colvin, T. S., and Cambardella, C. A.:
538 Nitrogen management strategies to reduce nitrate leaching in tile-drained Midwestern soils, *Agronomy*
539 *journal*, 94, 153-171, 2002.
- 540 Galloway, J. N., and Cowling, E. B.: Reactive nitrogen and the world: 200 years of change, *AMBIO: A*
541 *Journal of the Human Environment*, 31, 64-71, 2002.
- 542 Gast, R., Nelson, W., and Randall, G.: Nitrate accumulation in soils and loss in tile drainage following
543 nitrogen applications to continuous corn, *Journal of environmental quality*, 7, 258-261, 1978.
- 544 Harrison, R. M., Yamulki, S., Goulding, K., and Webster, C.: Effect of fertilizer application on NO and N₂O
545 fluxes from agricultural fields, *Journal of Geophysical Research: Atmospheres* (1984–2012), 100, 25923-
546 25931, 1995.



- 547 Hudman, R. C., Moore, N. E., Mebust, A. K., Martin, R. V., Russell, A. R., Valin, L. C., and Cohen, R. C.:
548 Steps towards a mechanistic model of global soil nitric oxide emissions: implementation and space
549 based-constraints, *Atmos. Chem. Phys.*, 12, 7779– 7795, doi:10.5194/acp-12-7779-2012, 2012. Hudman,
550 R. C., Russell, A. R., Valin, L. C., and Cohen, R. C.: Interannual variability in soil nitric oxide emissions over
551 the United States as viewed from space, *Atmos. Chem. Phys.*, 10, 9943– 9952, doi:10.5194/acp-10-9943-
552 2010, 2010.
- 553 IFIA: International Fertilizer Industry Association 2001. Nitrogen, phosphate and potash
554 statistics.(<http://www.fertilizer.org/ifa/statistics/IFADATA/dataline.asp>), 2001.
- 555 IPCC: Climate Change 2007: Impacts, Adaptation and Vulnerability, Contribution of Working Group II to
556 the Fourth Assessment Report of the Intergovernmental Panel on Climate Change, edited by: Parry, M.
557 L., Canziani, O. F., Palutikof, J. P., van der Linden, P. J., and Hanson, C. E., Cambridge University Press,
558 Cambridge, UK, 976 pp., 2007.
- 559 Jacob, D. I., and Bakwin, P. S.: Cycling of NO_x in tropical forest canopies, in *Microbial Production and*
560 *Consumption of Greenhouse Gases: Methane, Nitrogen Oxides and Halomethanes*, edited by J. E.
561 Rogers, and W. B. Whitman, pp. 237–253, *Am. Soc. of Microbiol.*, Washington, D. C., 1991.
- 562 Jaeglé, L., Martin, R. V., Chance, K., Steinberger, L., Kurosu, T. P., Jacob, D. J., Modi, A. I., Yoboué, V.,
563 Sigha-Nkamdjou, L., and Galy-Lacaux, C.: Satellite mapping of rain-induced nitric oxide emissions from
564 soils, *J. Geophys. Res.-Atmos.*, 109, D21310, doi:10.1029/2004JD004787, 2004.
- 565 Jaeglé, L., Steinberger, L., Martin, R. V., and Chance, K.: Global partitioning of NO_x sources using satellite
566 observations: Relative roles of fossil fuel combustion, biomass burning and soil emissions, *Faraday*
567 *Discussions*, 130, 407-423, 2005.
- 568 Kesik, M., Blagodatsky, S., Papen, H., and Butterbach-Bahl, K.: Effect of pH, temperature and substrate
569 on N₂O, NO and CO₂ production by *Alcaligenes faecalis* p, *Journal of applied microbiology*, 101, 655-
570 667, 2006.
- 571 Kottek, M., Grieser, J., Beck, C., Rudolf, B., and Rubel, F.: World Map of the Köppen-Geiger climate
572 classification updated. *Meteorologische Zeitschrift*, 15, 259-263. DOI: 10.1127/0941-2948/2006/0130,
573 2006.



- 574 Lamsal, L., Krotkov, N., Celarier, E., Swartz, W., Pickering, K., Bucsela, E., Gleason, J., Martin, R., Philip, S.,
575 and Irie, H.: Evaluation of OMI operational standard NO₂ column retrievals using in situ and surface-
576 based NO₂ observations, *Atmospheric Chemistry and Physics*, 14, 11587-11609, 2014.
- 577 Lin, J.-T.: Satellite constraint for emissions of nitrogen oxides from anthropogenic, lightning and soil
578 sources over East China on a high-resolution grid, *Atmospheric Chemistry and Physics*, 12, 2881-2898,
579 2012.
- 580 Liu, X., Ju, X., Zhang, Y., He, C., Kopsch, J., and Fusuo, Z.: Nitrogen deposition in agroecosystems in the
581 Beijing area, *Agriculture, ecosystems & environment*, 113, 370-377, 2006.
- 582 Ludwig, J., Meixner, F., Vogel, B., and Förstner, J.: Soil-air exchange of nitric oxide: an overview of
583 processes, environmental factors, and modeling studies, *Biogeochemistry*, 52, 225–257,
584 doi:10.1023/A:1006424330555, 2001.
- 585 Miyazaki, K., Eskes, H. J., and Sudo, K.: Global NO_x emission estimates derived from an assimilation of
586 OMI tropospheric NO₂ columns, *Atmos. Chem. Phys.*, 12, 2263–2288, doi:10.5194/acp-12-2263-2012,
587 2012.
- 588 Malm, W. C., Sisler, J. F., Huffman, D., Eldred, R. A., and Cahill, T. A.: Spatial and seasonal trends in
589 particle concentration and optical extinction in the United States, *JOURNAL OF GEOPHYSICAL*
590 *RESEARCH-ALL SERIES-*, 99, 1347-1347, 1994.
- 591 Otte, T. L. and Pleim, J. E.: The Meteorology-Chemistry Interface Processor (MCIP) for the CMAQ
592 modeling system: updates through MCIPv3.4.1, *Geosci. Model Dev.*, 3, 243-256, doi:10.5194/gmd-3-
593 243-2010, 2010.
- 594 Parton, W. J., Holland, E. A., Del Grosso, S. J., Hartman, M. D., Martin, R. E., Mosier, A. R., Ojima, D. S.,
595 and Schimel, D. S.: Generalized model for NO_x and N₂O emissions from soils, *J. Geophys. Res.-Atmos.*,
596 106, 17403–17419, doi:10.1029/2001JD900101, 2001.
- 597 Pilegaard, K.: Processes regulating nitric oxide emissions from soils, *Philosophical Transactions of the*
598 *Royal Society B: Biological Sciences*, 368, 20130126, 2013.
- 599 Pleim, J.E. and Xiu, A.: Development of a land surface model. Part II: Data assimilation. *Journal of*
600 *Applied Meteorology*, 42(12), pp.1811-1822, 2003.



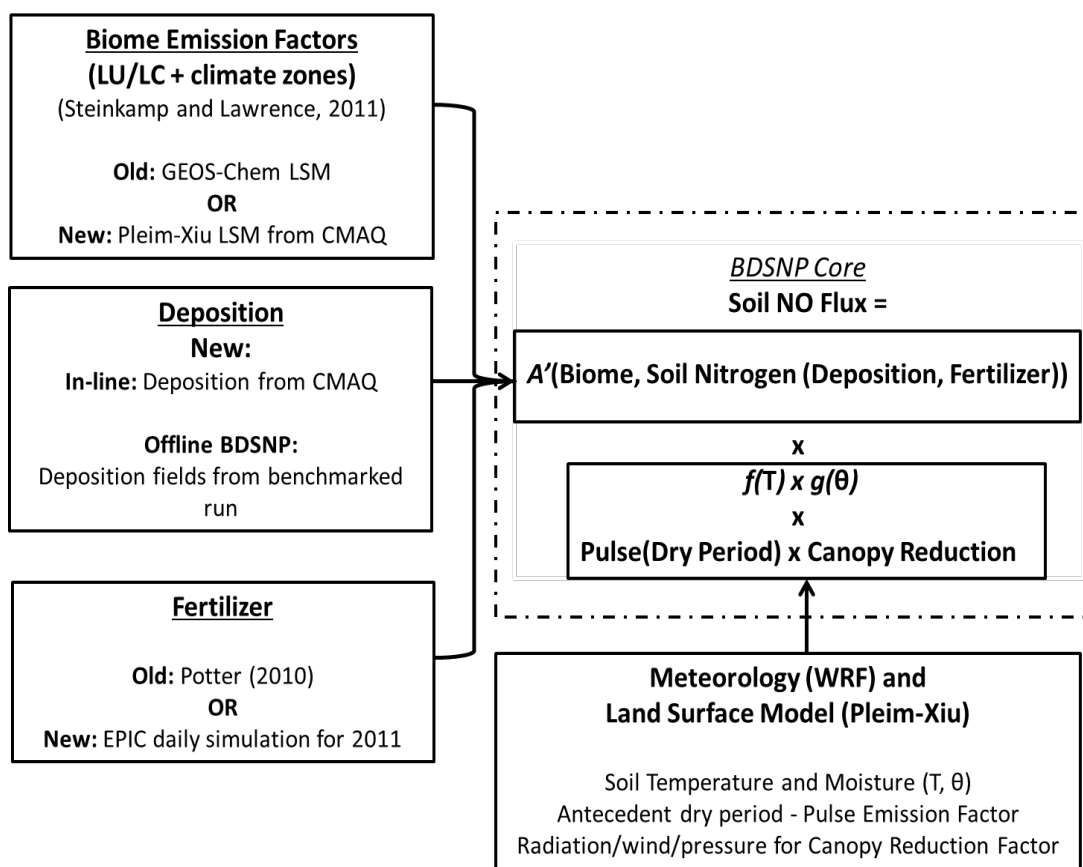
- 601 Potter, C., Matson, P., Vitousek, P., and Davidson, E.: Process modeling of controls on nitrogen trace gas
602 emissions from soils worldwide, *J. Geophys. Res.-Atmos.*, 101, 1361–1377, doi:10.1029/95JD02028,
603 1996.
- 604 Potter, P., Navin, R., Elena M. B., and Simon D. D.: Characterizing the spatial patterns of global fertilizer
605 application and manure production. *Earth Interactions*, 14, no. 2: 1-22, 2010.
- 606 Randall, G., Huggins, D., Russelle, M., Fuchs, D., Nelson, W., and Anderson, J.: Nitrate losses through
607 subsurface tile drainage in conservation reserve program, alfalfa, and row crop systems, *Journal of*
608 *Environmental Quality*, 26, 1240-1247, 1997.
- 609 Scholes, M., Martin, R., Scholes, R., Parsons, D., and Winstead, E.: NO and N₂O emissions from savanna
610 soils following the first simulated rains of the season, *Nutr. Cycl. Agroecosys.*, 48, 115– 122,
611 doi:10.1023/A:1009781420199, 1997.
- 612 Seinfeld, John H., and Spyros N. Pandis. *Atmospheric chemistry and physics: from air pollution to climate*
613 *change*. John Wiley & Sons, 2012.
- 614 Shepherd, M., Barzetti, S., and Hastie, D.: The production of atmospheric NO_x and N₂O from a
615 fertilized agricultural soil, *Atmospheric Environment. Part A. General Topics*, 25, 1961-1969, 1991.
- 616 Skamarock, W. C., Klemp, J. B., Dudhia, J., Gill, D. O., Barker, D. M., Duda, M. G., Huang, X., Wang, W.,
617 and Powers, J. G.: A description of the advanced research WRF version 3, NCAR Tech. Note, NCAR/TN-
618 475+STR, 8 pp., Natl. Cent. for Atmos. Res., Boulder, Colo., 2008 (available at:
619 http://www.mmm.ucar.edu/wrf/users/docs/arw_v3.pdf)
- 620 Stehfest, E., & Bouwman, L.: N₂O and NO emission from agricultural fields and soils under natural
621 vegetation: summarizing available measurement data and modeling of global annual emissions. *Nutrient*
622 *Cycling in Agroecosystems*, 74(3), 207-228. doi: 10.1007/s10705-006-9000-7, 2006.
- 623 Steinkamp, J., & Lawrence, M. G.: Improvement and evaluation of simulated global biogenic soil NO
624 emissions in an AC-GCM. *Atmospheric Chemistry and Physics*, 11(12), 6063–6082. doi:10.5194/acp-11-
625 6063-2011, 2011.
- 626 Stavrakou, T., Müller, J.-F., Boersma, K. F., De Smedt, I., and van der A, R. J.: Assessing the distribution
627 and growth rates of NO_x emission sources by inverting a 10 year record of NO₂ satellite columns,
628 *Geophys. Res. Lett.*, 35, L10801, doi:10.1029/2008GL033521, 2008.



- 629 Stavrakou, T., Müller, J.F., Boersma, K. F., van der A, R. J., Kurokawa, J., Ohara, T., and Zhang, Q.: Key
630 chemical NO_x sink uncertainties and how they influence top-down emissions of nitrogen oxides, Atmos.
631 Chem. Phys., 13, 9057–9082, doi:10.5194/acp-13-9057-2013, 2013.
- 632 Strode, S. A., Rodriguez, J. M., Logan, J. A., Cooper, O. R., Witte, J. C., Lamsal, L. N., Damon, M., Van
633 Aartsen, B., Steenrod, S. D., and Strahan, S. E.: Trends and variability in surface ozone over the United
634 States, J. Geophys. Res. Atmos., 120, 9020–9042, doi:10.1002/2014JD022784, 2015.
- 635 Su, H., Cheng, Y., Oswald, R., Behrendt, T., Trebs, I., Meixner, F. X., Andreae, M. O., Cheng, P., Zhang, Y.,
636 and Pöschl, U.: Soil nitrite as a source of atmospheric HONO and OH radicals, Science, 333, 1616-1618,
637 2011.
- 638 USDA ERS: USDA ERS (United States Department of Agriculture, Economic Research Service) Data sets:
639 U.S. fertilizer use and price. Last updated July 12, 2013. [http://www.ers.usda.gov/data-](http://www.ers.usda.gov/data-products/fertilizer-use-and-price.aspx)
640 [products/fertilizer-use-and-price.aspx](http://www.ers.usda.gov/data-products/fertilizer-use-and-price.aspx), 2013.
- 641 U.S. Environmental Protection Agency, Clean Air Markets Division, Clean Air Status and Trends Network
642 (CASTNET)[Ozone 8-Hour Daily Max] available at www.epa.gov/castnet. Date accessed: [July, 2011]
- 643 U.S. EPA : U.S. Environmental Protection Agency, 2015. Regulatory Impact Analysis of the Final
644 Revisions to the National Ambient Air Quality Standards for Ground-Level Ozone. EPA-452/R-15-007.
645 Office of Air Quality Planning and Standards, Research Triangle Park, NC. Last updated: March, 2016.
646 Available at: <https://www3.epa.gov/ttn/ecas/docs/20151001ria.pdf>.
- 647 van Dijk, S. M., A. Gut, G. A. Kirkman, B. M. Gomes, F. X. Meixner, and M. O. Andreae, Biogenic NO
648 emissions from forest and pasture soils: Relating laboratory studies to field measurements, J. Geophys.
649 Res., 107(D20), 8058, doi:10.1029/2001JD000358, 2002.
- 650 Veldkamp, E., and Keller, M.: Fertilizer-induced nitric oxide emissions from agricultural soils, Nutrient
651 Cycling in Agroecosystems, 48, 69-77, 1997.
- 652 Vinken, G. C. M., Boersma, K. F., Maasakkers, J. D., Adon, M., & Martin, R. V. (2014). Worldwide biogenic
653 soil NO_x emissions inferred from OMI NO₂ observations. Atmospheric Chemistry and Physics, 14(18),
654 10363–10381. doi:10.5194/acp-14-10363-2014.



- 655 Wang, Y., Logan, J. A., and Jacob, D. J.: Global simulation of tropospheric O₃-NO_x-hydrocarbon
656 chemistry: 2. Model evaluation and global ozone budget, *Journal of Geophysical Research: Atmospheres*
657 (1984–2012), 103, 10727-10755, 1998.
- 658 Wang, Y., McElroy, M. B., Martin, R. V., Streets, D. G., Zhang, Q., and Fu, T. M.: Seasonal variability of
659 NO_x emissions over east China constrained by satellite observations: Implications for combustion and
660 microbial sources, *Journal of Geophysical Research: Atmospheres* (1984–2012), 112, 2007.
- 661 Wang, Y., Zhang, Q. Q., He, K., Zhang, Q., and Chai, L.: Sulfate-nitrate-ammonium aerosols over China:
662 response to 2000–2015 emission changes of sulfur dioxide, nitrogen oxides, and ammonia, *Atmos.*
663 *Chem. Phys.*, 13, 2635-2652, doi:10.5194/acp-13-2635-2013, 2013.
- 664 Williams, E. J., Parrish, D. D., Buhr, M. P., Fehsenfeld, F. C., and Fall, R.: Measurement of soil NO_x
665 emissions in central Pennsylvania, *J. Geophys. Res.-Atmos.*, 93, 9539–9546,
666 doi:10.1029/JD093iD08p09539, 1988.
- 667 Williams, E. J., A. Guenther, F. C. Fehsenfeld, An inventory of nitric oxide emissions from soils in the
668 United States, *J. Geophys. Res.*, 97, 7511–7519, 1992.
- 669 Yienger, J., and Levy, H.: Empirical model of global soil-biogenic NO_x emissions, *JOURNAL OF*
670 *GEOPHYSICAL RESEARCH-ALL SERIES-*, 100, 11,447-411,447, 1995.
- 671 Zhang, W., Mo, J., Yu, G., Fang, Y., Li, D., Lu, X., and Wang, H.: Emissions of nitrous oxide from three
672 tropical forests in Southern China in response to simulated nitrogen deposition, *Plant and Soil*, 306, 221-
673 236, 2008.
- 674 Zhang, Y., Dulière, V., Mote, P.W. and Salathé Jr, E.P.: Evaluation of WRF and HadRM mesoscale climate
675 simulations over the US Pacific Northwest*. *Journal of Climate*, 22(20), pp.5511-5526, 2009.
- 676 Zhang, L., Jacob, D. J., Knipping, E. M., Kumar, N., Munger, J. W., Carouge, C. C., van Donkelaar, A.,
677 Wang, Y. X., and Chen, D.: Nitrogen deposition to the United States: distribution, sources, and processes,
678 *Atmos. Chem. Phys.*, 12, 4539–4554, doi:10.5194/acp-12-4539-2012, 2012.
- 679 Zhao, C., and Wang, Y.: Assimilated inversion of NO_x emissions over East Asia using OMI NO₂ column
680 measurements, *Geophysical Research Letters*, 36, 2009.

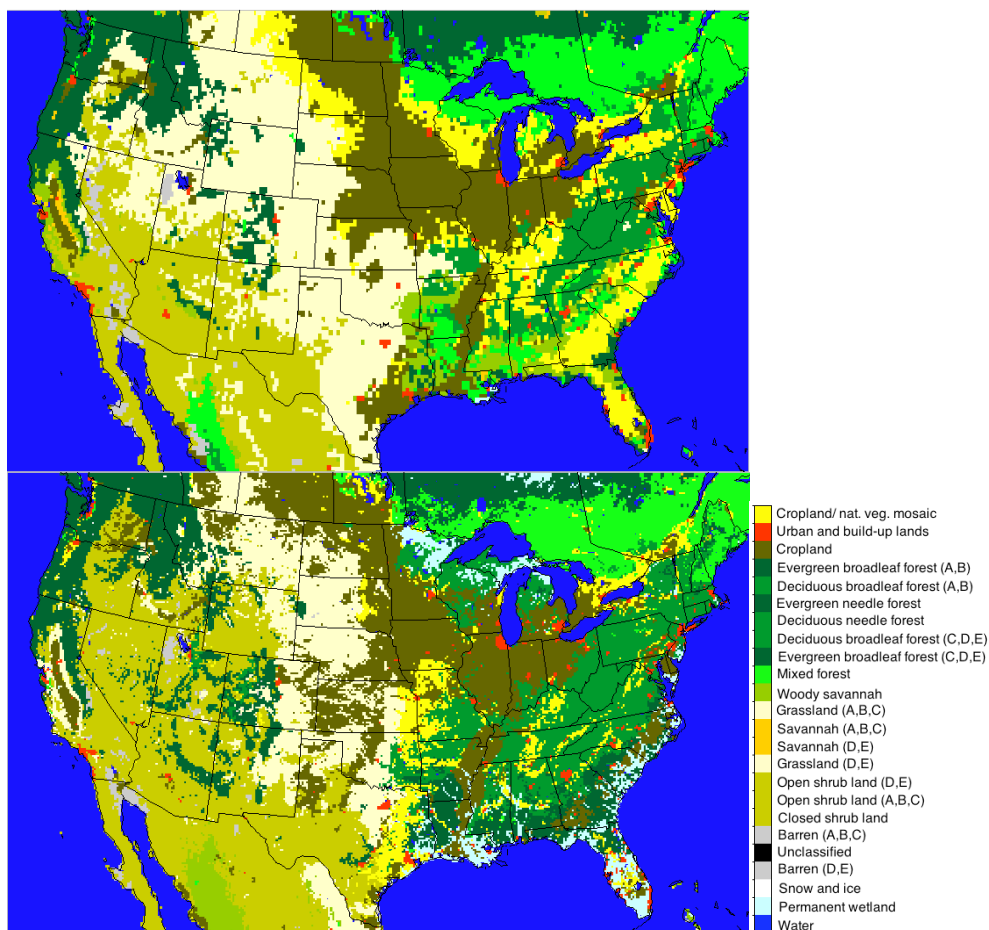


681
 682
 683
 684
 685
 686
 687

Figure 1 Soil NO emissions modeling framework as implemented offline or in CMAQ (inline). “Old” refers to the Hudman et al. (2012) implementation in GEOS-Chem. “New” refers to our implementation in CMAQ.



688



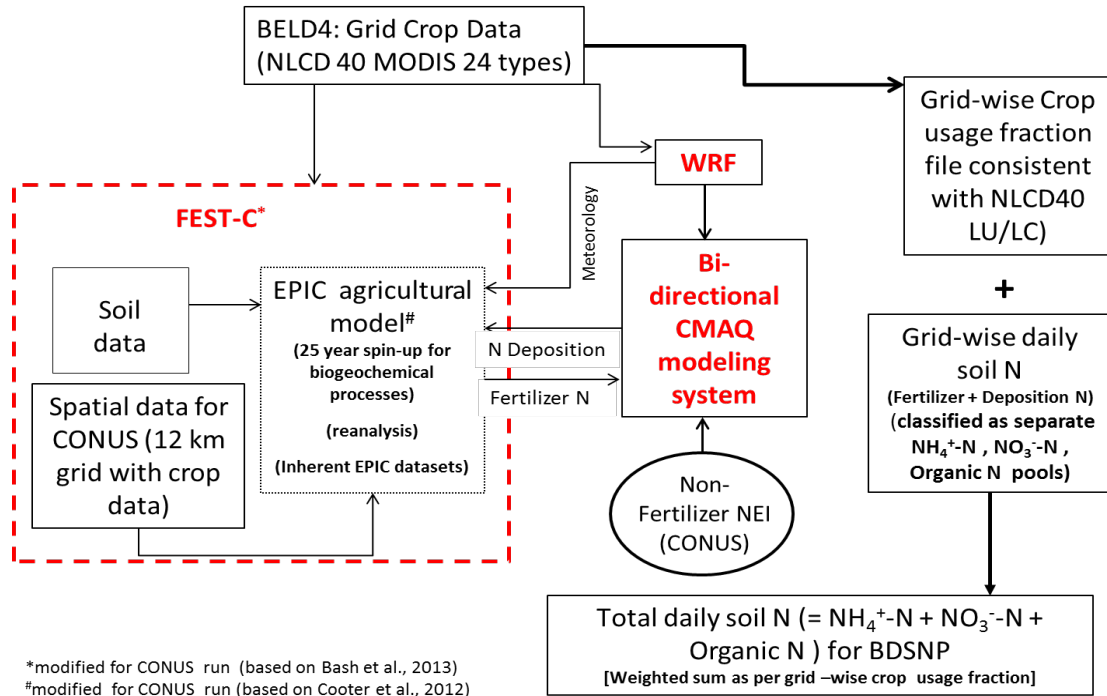
689

690 **Figure 2** Biomes from GEOS-Chem ($0.25^\circ \times 0.25^\circ$; top) and CMAQ MODIS NLCD40 (12 km x
691 12 km; bottom) regrouped to match the classifications for which emission factors are available
692 from Steinkamp and Lawrence (2011). See Tables A1 and A2 (right) for the mappings between
693 classifications. The color-bar legends for classifications are as per NLCD definitions
694 (http://www.mrlc.gov/nlcd11_leg.php).

695

696

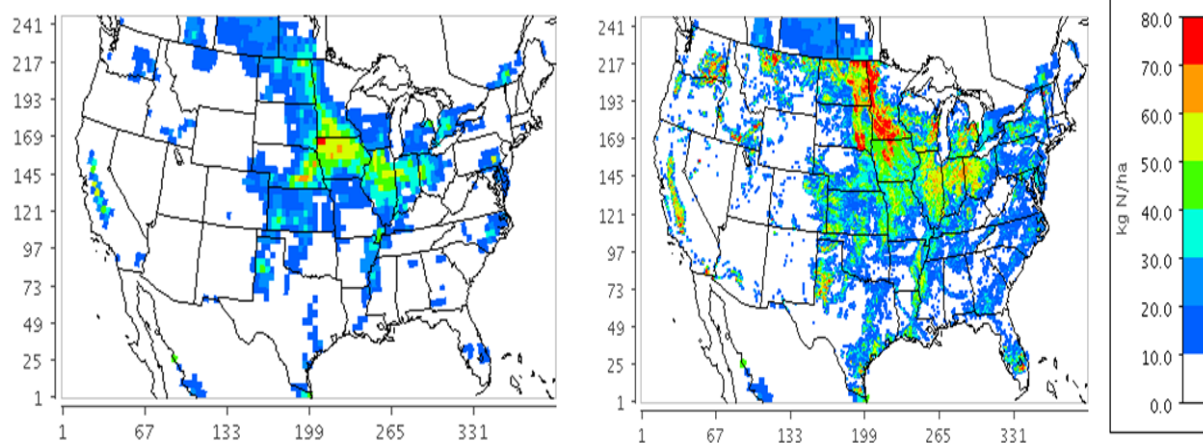
697



698

699 **Figure 3** Modeling framework for obtaining total soil N from EPIC using FEST-C.

700



701

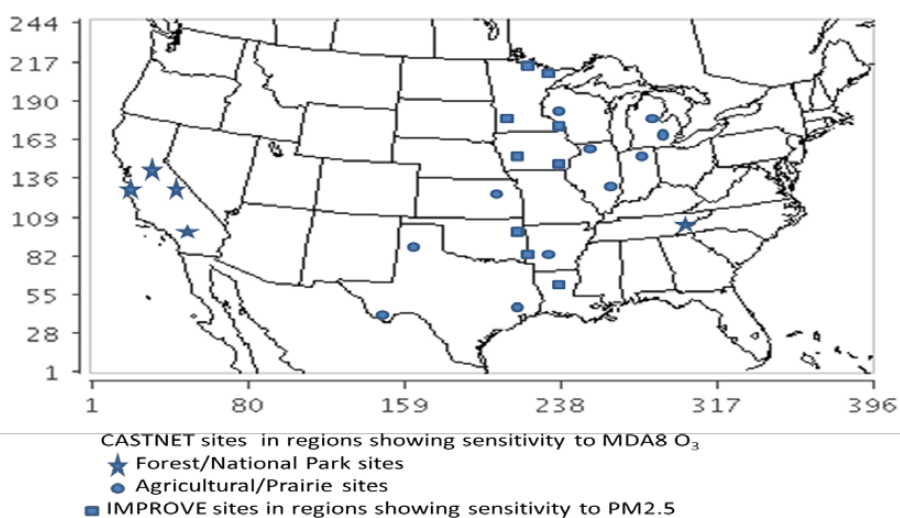
Min (1, 1) = 0.0, Max (209, 164) = 76.8

702

Figure 4 Potter (left) and EPIC (right) annual fertilizer application (Kg N/ha). Since EPIC
703 modeled only the U.S., Potter et al. (2010) is used in both cases to represent Canada and Mexico.

704

Min (1, 1) = 0.0, Max (207, 211) = 115.5



705

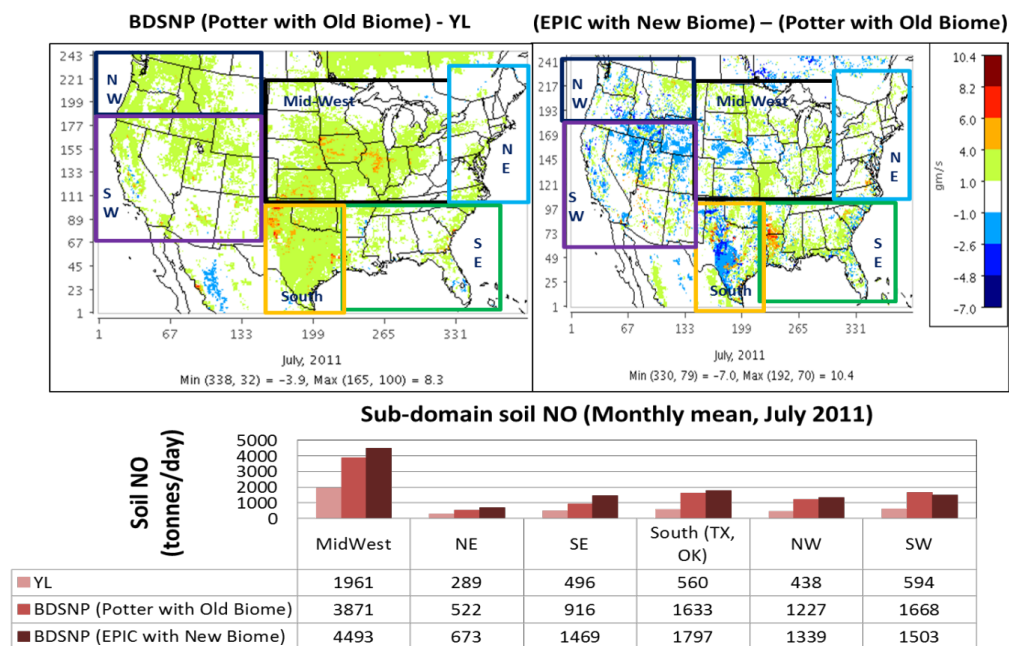
706 **Figure 5** CASTNET (Forest/National Park and agricultural sites) and IMPROVE sites in
707 continental US for comparison of modeled and observed ozone and PM_{2.5}.

708

709

710

711



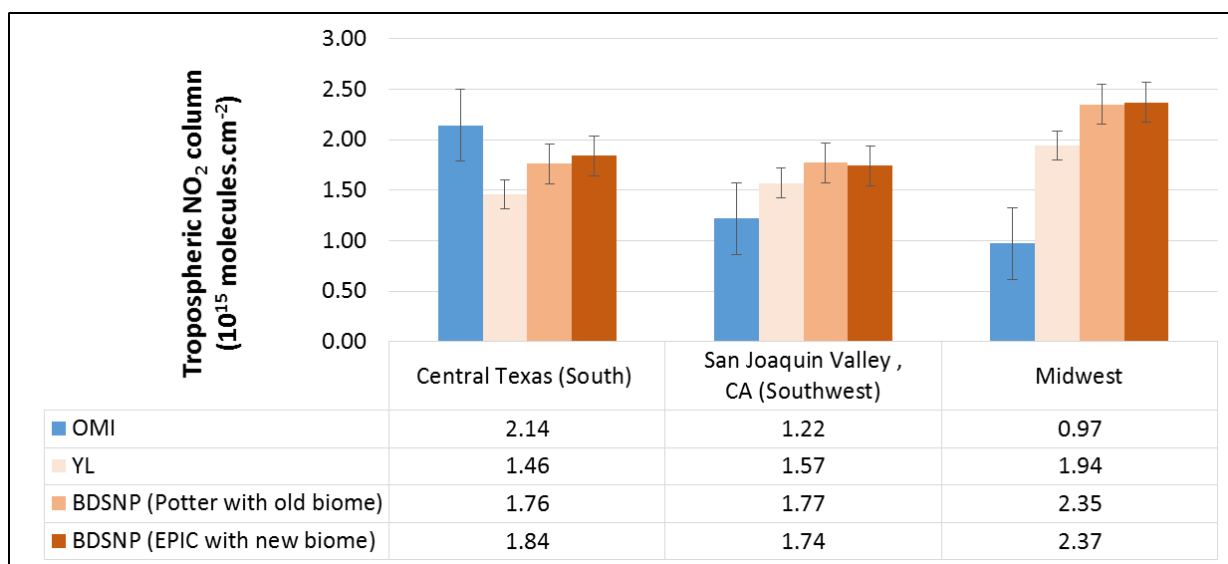
712

713 **Figure 6** Soil NO (tonnes/day) sensitivity to change from YL to BDSNP (Potter and old biome
 714 or 'old') (left) and to the fertilizer and biome scheme within BDSNP (right) over sub-domains
 715 (boxes).

716



717



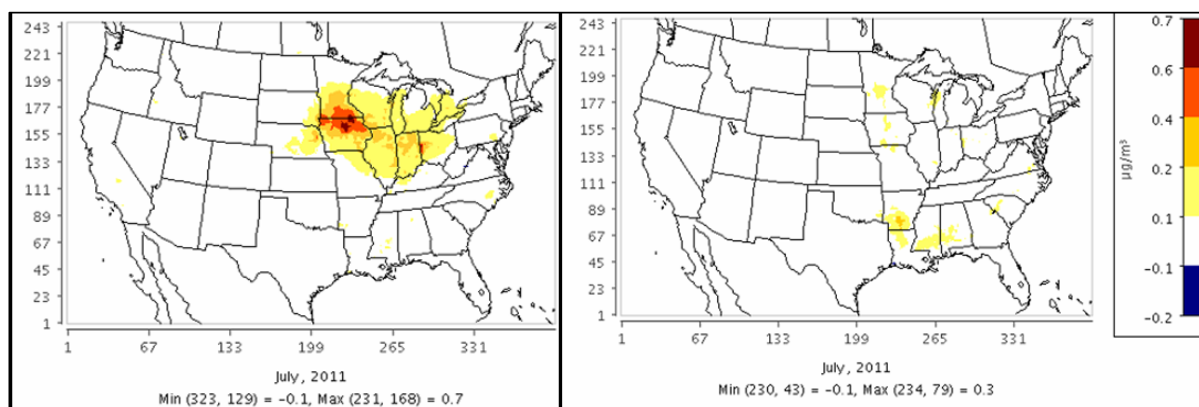
718

719 **Figure 7** Spatial average for Tropospheric NO₂ (molecules cm⁻²) over regions with high soil NO
 720 sensitivity with switch from YL to BDSNP (as in Figure 6) with comparison to OMI NO₂. NO₂
 721 column are temporal average for July 2011 at OMI overpass time.

722



723

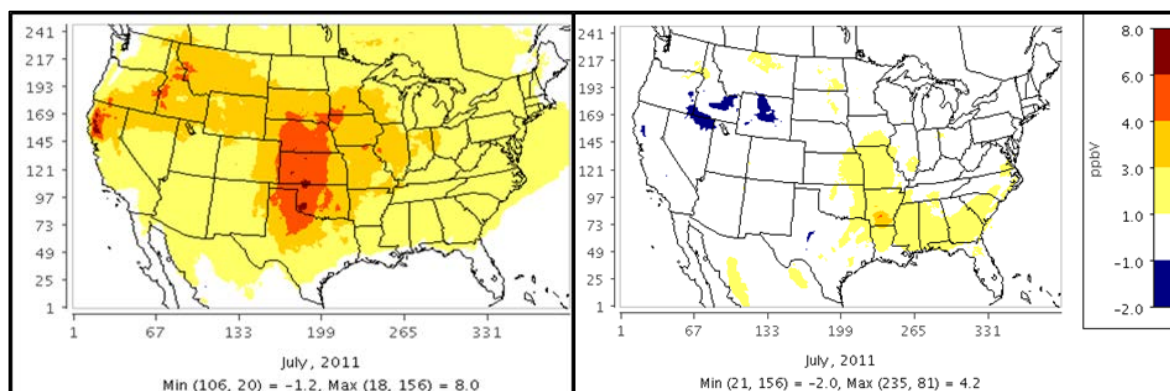


724

725 **Figure 8** Changes in modeled daily average $PM_{2.5}$ when switching from: a) YL to BDSNP
 726 (Potter fertilizer data with original biome map) (left) and b) BDSNP (Potter with original
 727 biomes) to BDSNP (EPIC with new biomes) (right).

728

729



730

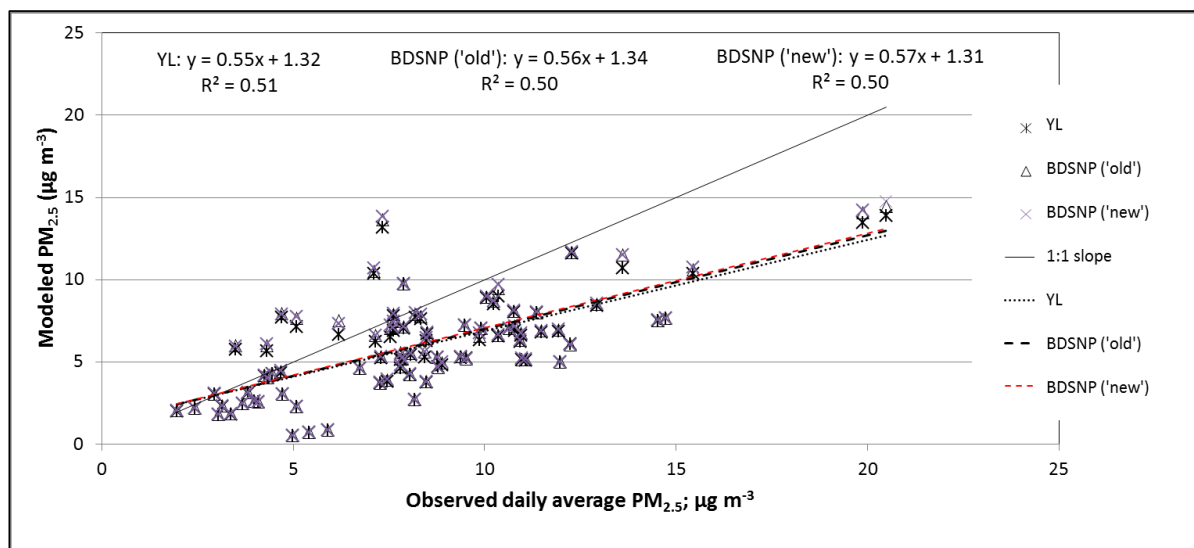
731 **Figure 9** Changes in modeled maximum daily 8-hour ozone (MDA8) when switching from: a)
 732 YL to BDSNP (Potter fertilizer data with original biome map) (left) and b) BDSNP (Potter with
 733 original biomes) to BDSNP (EPIC with new biomes) (right).

734



735

736



737

738 **Figure 10** Comparison of the three inline BDSNP-CMAQ cases with IMPROVE PM_{2.5} data
739 (Malm et al., 1994) in continental US for Daily Average PM_{2.5} for July 2011.

740

741

742

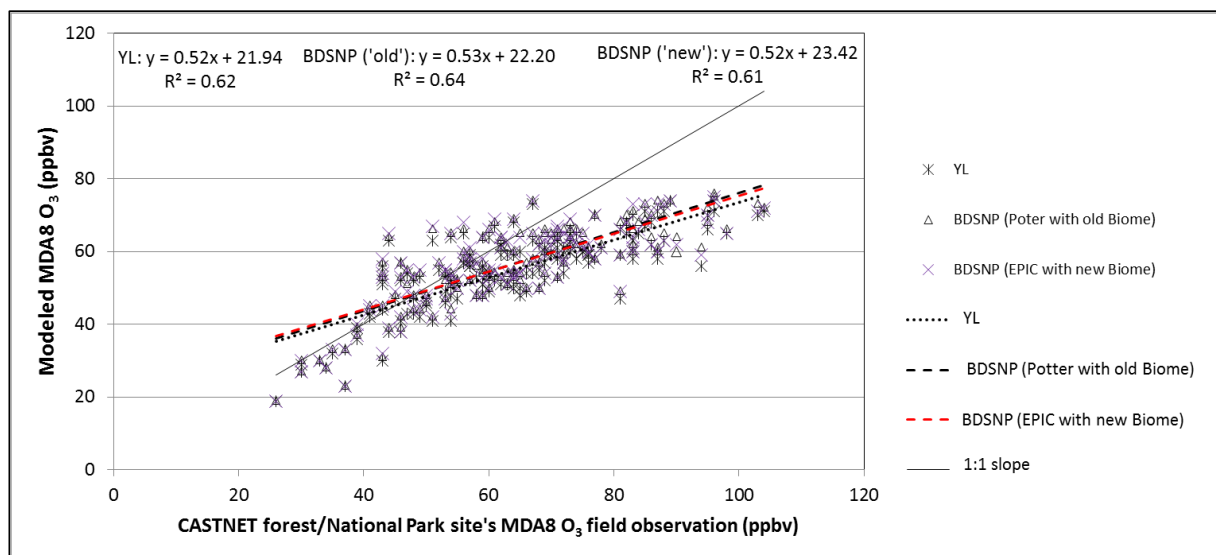
743

744

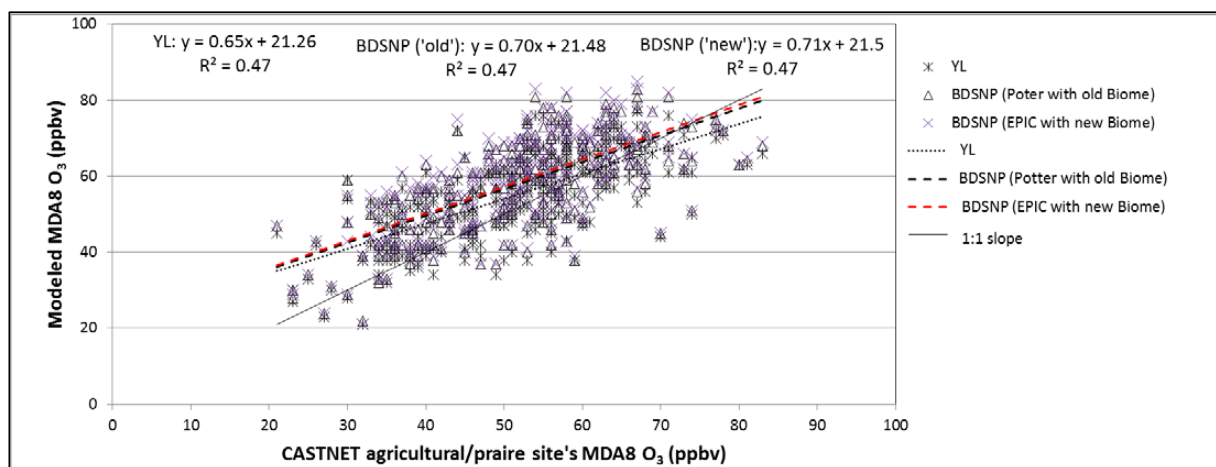
745



746

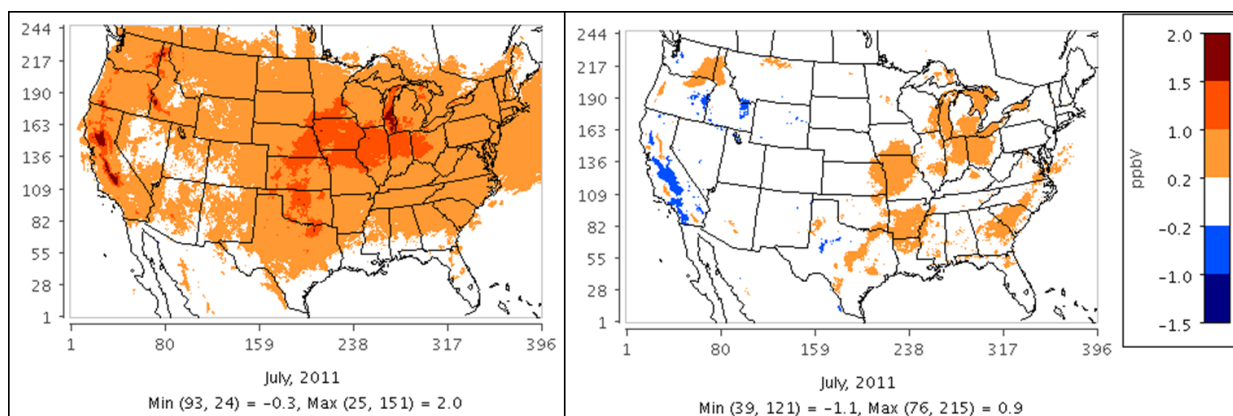


747



748 **Figure 11** Comparison of the three inline BDSNP-CMAQ cases with CASTNET MDA8 O₃ data
 749 for forest/National Park sites in California (top, number of evaluation sites, n=147) and
 750 agricultural/prairie sites in mid-west and south US (bottom, n=311) for July 2011.

751



752

753 **Figure 12** Difference in monthly mean MDA8 O₃ perturbation between: a) BDSNP ('old') –
754 YL (left) and, b) BDSNP ('new') – BDSNP ('old') (right). MDA8 O₃ perturbations are from
755 perturbed anthropogenic NO_x estimates 2011 base case to 2025 base case, BAU (US EPA,
756 2015).

757

758

759

760

761

762

763

764

765

766

767

768

769

770



771 **Table 1** Modeling configuration used for the WRF-BDSNP-CMAQ CONUS domain runs.

WRF/MCIP			
Version:	ARW V3.6.1	Shortwave radiation:	RRTMG scheme
Horizontal resolution:	CONUS (12kmX12km)	Surface layer physic:	Pleim-Xiu surface model
Vertical resolution:	26 layer	PBL scheme:	ACM2
Boundary condition:	NARR 32km	Microphysics:	Morrison double-moment scheme
Initial condition:	NCEP-ADP	Cumulus parameterization:	Kain-Fritsch scheme
Longwave radiation:	RRTMG scheme	Assimilation:	Analysis nudging above PBL for temperature, moisture and wind speed
BDSNP			
Horizontal resolution:	Same as WRF/MCIP	Emission factor:	Steinkamp and Lawrence (2011)
Soil Biome type:	24 types based on NLCD40 (new) 24 types based on GEOS-Chem LSM (old)	Fertilizer database:	EPIC 2011 based from FEST-C (new) Potter et al. (2010) (old)
CMAQ			
Version:	V5.02	Anthropogenic emission:	NEI2011
Horizontal resolution:	Same as WRF/MCIP	Biogenic emission:	BEIS V3.1 in-line
Initial condition:	Pleim-Xiu (new) GEOS-Chem (old)	Boundary condition:	Pleim-Xiu (new) GEOS-Chem (old)
Aerosol module:	AE5	Gas-phase mechanism:	CB-05
Simulation Case Arrangement (in-line with CMAQ)			
1. YL:	WRF/MCIP-CMAQ with standard YL soil NO scheme		
2. BDSNP (Potter with old Biome or 'old'):	WRF/MCIP-BDSNP-CMAQ with Potter and old biome		
3. BDSNP (EPIC with new Biome or 'new'):	WRF/MCIP-BDSNP-CMAQ with EPIC and new biome		
Simulation Time Period			
July 1-31, 2011 for CMAQ simulation with in-line soil NO BDSNP module Daily simulations in Year 2011 for standalone BDSNP soil NO BDSNP module (July 1-31, 2011 for sensitivity analysis)			
Model Performance Evaluation			
USEPA Clean Air Status and Trends Network (CASTNET) data for MDA8 ozone Interagency Monitoring of Protected Visual Environments (IMPROVE) Network (Malm et al., 1994) for PM _{2.5} OMI NO ₂ satellite retrieval product as derived in Lamsal et al., 2014 for NO ₂ column			



773 **Table 2** Aggregated performance statistics of CMAQ modeled daily average PM_{2.5} for stations
774 showing sensitivities with change in soil NO between YL scheme and our 2 inline BDSNP
775 implementations (‘old’ and ‘new’) for CONUS in July 2011 as compared to observations at these
776 sites

		Metrics		
		Sample Size	81	
		Mean observed (µg/m ³)	8.26	
			BDSNP	BDSNP
		3 CMAQ inline cases	(Potter with old biome)	(EPIC with new biome)
		YL		
Daily average	Mean predicted (µg/m ³)	5.91	6.04	6.08
PM _{2.5} July (1 July- 31 July), 2011	MAGE (Mean Absolute Gross error)	2.86	2.80	2.77
	RMSE	3.45	3.40	3.38
	R	0.72	0.71	0.71
	(correlation coefficient)			
	Spearman’s Ranked	0.65	0.63	0.63
	NMB (%)	-28.52	-26.90	-26.44
	NME (%)	34.64	33.88	33.57

777

778

779



780 **Table 3** Performance statistics of CMAQ modeled MDA8 Ozone for 16 CASTNET remote sites
 781 grouped into two categories: a) 11 sites with moist or wet soil condition (monthly mean soil
 782 moisture (m^3/m^3), $\theta_{\text{mean}} > 0.175$), and b) 5 sites with dry soil condition ($\theta_{\text{mean}} < 0.175$), using soil
 783 NO from YL and our two inline BDSNP schemes.

July 2011		Metrics			
		Sample size		311	
		Mean observed (ppbv)		51.76	
		3 CMAQ inline cases	YL	BDSNP (Potter with old biome)	BDSNP (EPIC with new biome)
11 CASTNET sites (mostly agricultural/prairie sites, Mostly wet soil conditions)	Mean modeled (ppbv)	55.25	57.93	58.60	
	M_{AGE} (Mean Absolute Gross error)	7.78	9.16	9.65	
	RMSE	9.41	10.96	11.47	
	R	Pearson's	0.50	0.51	0.50
	(correlation coefficient)	Spearman's Ranked	0.46	0.49	0.48
	NMB (%)		7.57	12.80	14.08
	NME (%)		15.65	18.38	19.33
		Sample size		147	
		Mean observed (ppbv)		64.38	
5 CASTNET sites (mostly forest/National Park sites near San Joaquin valley CA, Dry soil conditions)	Mean modeled (ppbv)	55.17	57.01	56.87	
	M_{AGE} (Mean Absolute Gross error)	11.41	10.13	10.44	
	RMSE	13.13	11.80	12.12	
	R	Pearson's	0.71	0.72	0.72
	(correlation coefficient)	Spearman's Ranked	0.68	0.69	0.69
	NMB (%)		-13.14	-10.23	-10.35
	NME (%)		16.95	15.04	15.45



785 **Table 4** Emission perturbation factors applied to anthropogenic NO_x emissions for each sector
 786 listed in NEI as per EPA's RIA base-line reductions from 2011 to 2025 with BAU (Table 2A-1,
 787 <https://www3.epa.gov/ttn/ecas/docs/20151001ria.pdf>)

Sectors (NEI file names)	Perturbation factor
Electric Generating Unit(EGU)-point (ptimp- ptegu, ptegu_pk)	0.7
NonEGU-point (ptnonipm)	1
Point oil and gas (pt_oilgas)	0.92
Nonpoint oil and gas (np_oilgas)	1.108
Wild and Prescribed Fires (ptwildfire, ptprescfire)	1
Residential wood combustion (rwc)	1.029
Other nonpoint (nonpt)	1.039
Onroad (onroad)	0.298
Nonroad mobile equipment sources (nonroad)	0.5
Category 3 Commercial marine vessel (c3marine)	0.77
Locomotive and Category 1/Category 2 Commercial marine vessel (c1c2rail)	0.62

788

789

790

791

792

793

794



795 **Appendix**

796 **Table A1** List of 24 soil biome emission factor (EF) from Steinkamp and Lawrence (2010)

ID	MODIS land cover	Köppen main climate ⁽¹⁾	EF1 (world geometric mean)	EF2 (world arithmetic mean)	EF3 (North American)
1	Water	--	0	0	0
2	Permanent wetland	--	0	0	0
3	Snow and ice	--	0	0	0
4	Barren	D,E	0	0	0
5	Unclassified	--	0	0	0
6	Barren	A,B,C	0.06	0.06	0.06
7	Closed shrub land	--	0.09	0.21	0.05
8	Open shrub land	A,B,C	0.09	0.21	0.09
9	Open shrub land	D,E	0.01	0.01	0.01
10	Grassland	D,E	0.84	1.05	0.62
11	Savannah	D,E	0.84	1.05	0.84
12	Savannah	A,B,C	0.24	0.97	0.24
13	Grassland	A,B,C	0.42	1.78	0.37
14	Woody savannah	--	0.62	0.74	0.62
15	Mixed forest	--	0.03	0.14	0.00
16	Evergreen broadleaf forest	C,D,E	0.36	0.95	0.36
17	Deciduous broadleaf forest	C,D,E	0.36	0.95	0.61
18	Deciduous needle. forest	--	0.35	0.95	0.35
19	Evergreen needle. forest	--	1.66	4.60	1.66
20	Deciduous. broadl. forest	A,B	0.08	0.13	0.08
21	Evergreen broadl. forest	A,B	0.44	1.14	0.44
22	Cropland	--	0.57	3.13	0.33
23	Urban and build-up lands	--	0.57	3.13	0.57
24	Cropland/nat. veg. mosaic	--	0.57	3.14	0.57

797 (1). A-equatorial, B-arid, C-warm temperature, D-snow, E-polar (see Figure 2 for spatial map)

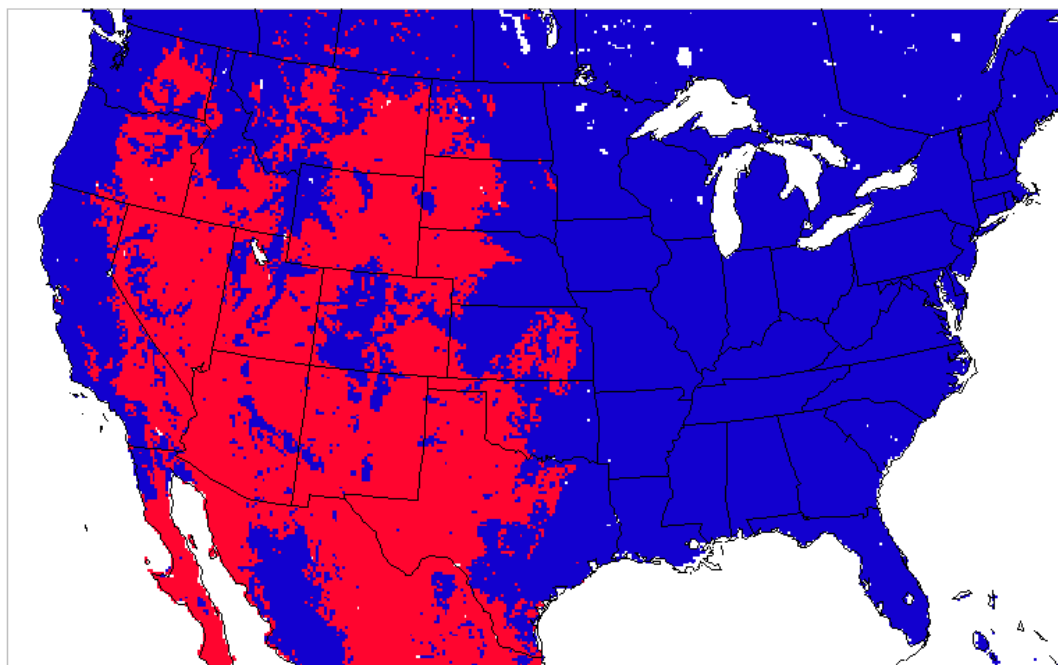
798

799



800 **Table A2** Mapping table to create the ‘new’ soil biome map based on NLCD40 MODIS land
 801 cover categories

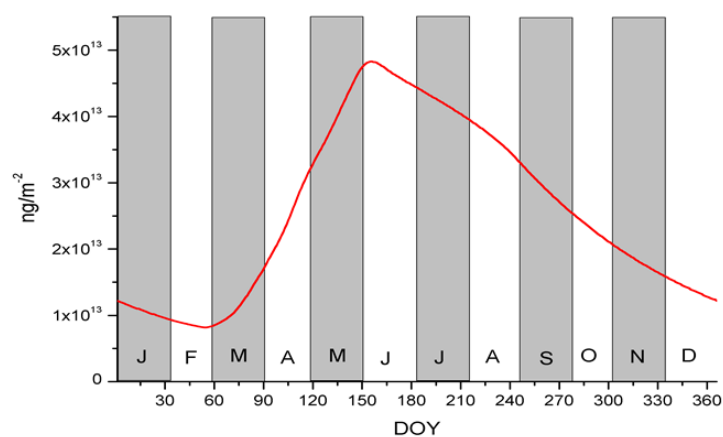
ID	NLCD40 MODIS CATEGORY (40)	ID	SOIL BIOME CATEGORY (24)
1	Evergreen Needle leaf Forest	19	Evergreen Needle leaf Forest
2	Evergreen Broadleaf Forest	16 and 21	Evergreen Broadleaf Forest
3	Deciduous Needle leaf Forest	18	Dec. Needle leaf Forest
4	Deciduous Broadleaf Forest	17 and 20	Dec. Broadleaf Forest
5	Mixed Forests	15	Mixed Forest
6	Closed shrublands	7	Closed shrublands
7	Open shrublands	8 and 9	Open shrublands
8	Woody Savannas	14	Woody savannah
9	Savannas	11 and 12	Savannah
10	Grasslands	10 and 13	Grassland
11	Permanent Wetlands	2	Permanent Wetland
12	Croplands	22	Cropland
13	Urban and Built Up	23	Urban and build-up lands
14	Cropland-Natural Vegetation Mosaic	24	Cropland/nat. veg. mosaic
15	Permanent Snow and Ice	3	Snow and ice
16	Barren or Sparsely Vegetated	6	Barren
17	IGBP Water	1	Water
18	Unclassified	1	Water
19	Fill value	1	Water
20	Open Water	1	Water
21	Perennial Ice-Snow	3	Snow and ice
22	Developed Open Space	23	Urban and build-up lands
23	Developed Low Intensity	23	Urban and build-up lands
24	Developed Medium Intensity	23	Urban and build-up lands
25	Developed High Intensity	23	Urban and build-up lands
26	Barren Land (Rock-Sand-Clay)	24	Cropland/nat. veg. mosaic
27	Unconsolidated Shore	24	Cropland/nat. veg. mosaic
28	Deciduous Forest	16 and 21	Evergreen Broadleaf Forest
29	Evergreen Forest	19	Evergreen Needle leaf Forest
30	Mixed Forest	15	Mixed Forest
31	Dwarf Scrub	8 and 9	Open shrublands
32	Shrub-Scrub	8 and 9	Open shrubland
33	Grassland-Herbaceous	10 and 13	Grassland
34	Sedge-Herbaceous	14	Woody savannah
35	Lichens	10 and 13	Grassland
36	Moss	10 and 13	Grassland
37	Pasture-Hay	24	Cropland/nat. veg. mosaic
38	Cultivated Crops	22	Cropland
39	Woody Wetlands	2	Permanent Wetland
40	Emergent Herbaceous Wetlands	2	Permanent Wetland



803

804 **Figure B1** Arid (red) and non-arid (blue) region over Continental US (12km resolution)

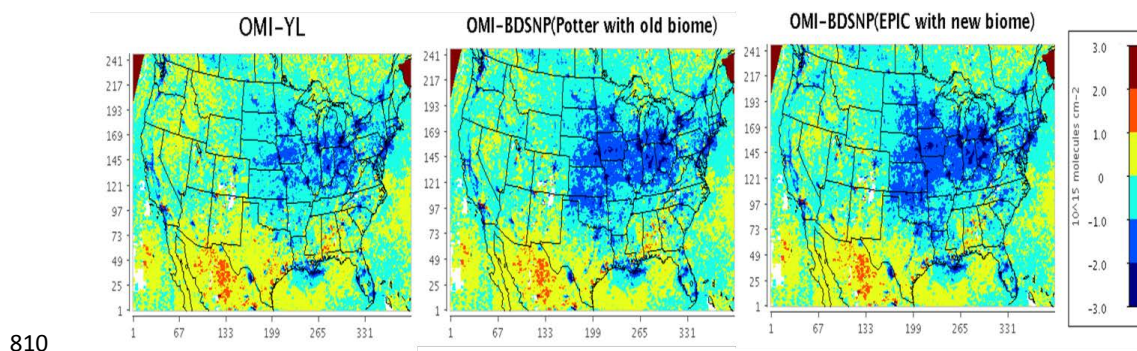
805



806

807 **Figure B2** Daily variation of total N from fertilizer application (from Potter et al. (2010))
808 processed from BDSNP to establish timing over continental US throughout 2011

809



810

811 **Figure B3** Difference of OMI NO₂ column with NO₂ column simulated from the three inline
812 CMAQ cases: YL, BDSNP (Potter with old biome), BDSNP (EPIC with new Biome) (left to
813 right) over OMI overpass time averaged for July 2011 over CONUS. Note: In contour plots,
814 white refers to gaps/no-fill values in OMI product and dark red at upper corners are due to gaps
815 in CMAQ NO₂ column after temporal averaging at OMI overpass time.